Synergistic action of WDR5 and HDM2 inhibitors in SMARCB1-deficient cancer cells

Andrea C. Florian [1], Chase M. Woodley[1], Jing Wang[2,3], Brian C. Grieb[1,4], Macey J. Slota[1], Kiana Guerrazzi[1], Chih-Yuan Hsu[2,3], Brittany K. Matlock[5], David K. Flaherty[5], Shelly L. Lorey[1], Stephen W. Fesik[6,7,8], Gregory C. Howard[1], Qi Liu[2,3], April M. Weissmiller[1,*] and William P. Tansey [1,6,*]

[1]Department of Cell and Developmental Biology, Vanderbilt University School of Medicine, Nashville, TN 37232, USA, [2]Department of Biostatistics, Vanderbilt University Medical Center, Nashville, TN 37232, USA, [3]Center for Quantitative Sciences, Vanderbilt University Medical Center, Nashville, TN 37232, USA, [4]Department of Medicine, Vanderbilt University Medical Center, Nashville, TN 37232, USA, [5]Vanderbilt University Medical Center Flow Cytometry Shared Resource, Vanderbilt University Medical Center, Nashville, TN 37240, USA, [6]Department of Biochemistry, Vanderbilt University School of Medicine, Nashville, TN 37232, USA, [7]Department of Pharmacology, Vanderbilt University School of Medicine, Nashville, TN 37232, USA and [8]Department of Chemistry, Vanderbilt University School of Medicine, Nashville, TN 37232, USA

ABSTRACT

Rhabdoid tumors (RT) are rare and deadly pediatric cancers driven by loss of *SMARCB1*, which encodes the SNF5 component of the SWI/SNF chromatin remodeler. Loss of *SMARCB1* is associated with a complex set of phenotypic changes including vulnerability to inhibitors of protein synthesis and of the p53 ubiquitin-ligase HDM2. Recently, we discovered small molecule inhibitors of the 'WIN' site of WDR5, which in MLL-rearranged leukemia cells decrease the expression of a set of genes linked to protein synthesis, inducing a translational choke and causing p53-dependent inhibition of proliferation. Here, we characterize how WIN site inhibitors act in RT cells. As in leukemia cells, WIN site inhibition in RT cells causes the comprehensive displacement of WDR5 from chromatin, resulting in a decrease in protein synthesis gene expression. Unlike leukemia cells, however, the growth response of RT cells to WIN site blockade is independent of p53. Exploiting this observation, we demonstrate that WIN site inhibitor synergizes with an HDM2 antagonist to induce p53 and block RT cell proliferation *in vitro*. These data reveal a p53-independent action of WIN site inhibitors and forecast that future strategies to treat RT could be based on dual WDR5/HDM2 inhibition.

GRAPHICAL ABSTRACT

Rhabdoid Tumor Cells
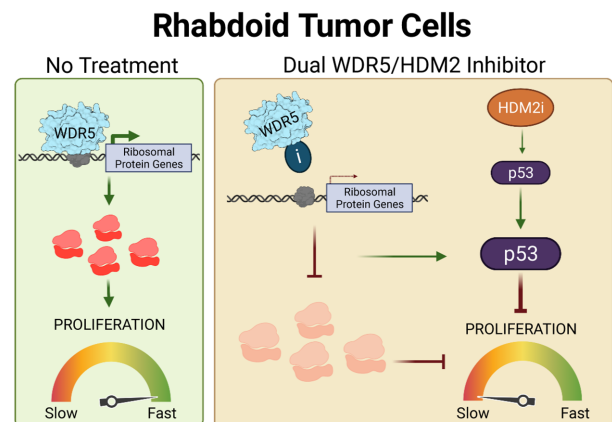
INTRODUCTION

Rhabdoid tumors are rare cancers that affect children under the age of two ([1]). Presenting as cancers in the brain, where they are termed atypical teratoid/rhabdoid tumor (AT/RT), or elsewhere in the body, where they are termed malignant rhabdoid tumor (MRT), these tumors spread quickly and are often fatal ([2]). Some improvements in patient survival have been made in recent years ([2]), but there are few effective treatment options for rhabdoid tumors (RT), and despite regimens that can involve combinations of surgery, chemotherapy, and radiation, most children with RT die within 18 months ([1]). Indeed, the five year survival

*To whom correspondence should be addressed. William P. Tansey. Tel: +1 615 322 1993; Email: william.p.tansey@vanderbilt.edu
Correspondence may also be addressed to April M. Weissmiller. Tel: +1 615 898 5868; Email: april.weissmiller@mtsu.edu
Present address: April M. Weissmiller, Department of Biology, Middle Tennessee State University, Murfreesboro, TN 32132, USA.

rate of children diagnosed with RT is 20% ([1]), highlighting the need for new targeted therapies that can substantively improve RT patient outcomes.

One remarkable facet of MRT and AT/RT is that they have an uncommonly simple genetic profile, defined by deficits in a single gene, *SMARCB1* ([3–5]), which encodes the SNF5 component of the SWI/SNF chromatin remodeling complex. Loss of *SMARCB1* is the only recurring mutation in these cancers, and often the only mutation detected in RT genomes ([5]). Haploinsufficiency for *SMARCB1* predisposes to rhabdoid tumors *in vivo* ([6]), and reintroduction of SNF5 into patient-derived cell lines induces cell cycle arrest, apoptosis, and reversal of tumorigenicity ([7])—demonstrating that SNF5 loss is causing and sustaining the rhabdoid tumor state.

Although RT is unusual among malignancies in that it has a singular genetic basis, recent work has demonstrated that loss of SNF5 is associated with a complex set of molecular and phenotypic changes. The absence of SNF5 compromises SWI/SNF expression and integrity ([8]), resulting in loss of bivalent promoter activation ([9]), collapse of enhancers regulating differentiation ([8–10]), and mobilization of 'residual' SWI/SNF complexes to super-enhancers and promoters that are essential for tumor maintenance ([8,9]). Additionally, SNF5 loss promotes the function of a BRD9-containing SWI/SNF subcomplex that is required for survival of *SMARCB1*-deficient RT cells ([11,12]). Loss of SNF5 further enables enhanced access of the oncoprotein c-MYC to its transcriptional targets ([13,14]), a phenomenon presumably responsible for the recurrent activation of MYC target gene signatures in *SMARCB1*-null cancers ([15–17]). At the cellular level, SNF5 deficiency induces ER stress and the unfolded protein response via the MYC–p19ARF–p53 axis ([18]), a process that protects RT cells from proteotoxic cell death and could explain the near-universal retention of wild-type *TP53* in RT genomes ([19]). Together, these studies highlight the processes that go awry in RT cells, and identify a number of actionable strategies that could be pursued to develop therapies against these deadly cancers.

Recently, we reported discovery of potent small molecule inhibitors of WDR5 ([20–22]), a chromatin-associated protein with numerous links to tumorigenesis. WDR5 is overexpressed in multiple cancers, and is a promising pharmacological target in malignancies driven by MLL1 fusions, C/EBPα p30, p53 gain-of-function mutants, and MYC ([23]). Its best understood role is scaffolding assembly of the MLL/SET histone methyltransferase complexes that catalyze histone H3 lysine 4 methylation, but WDR5 also 'moonlights' in other molecular processes, both on and off chromatin ([23]). Notably, WDR5 is important for controlling the expression of a set of genes linked to protein synthesis, including half of the ribosomal protein genes (RPGs), as well as those encoding translation factors and nucleolar RNAs ([24]). WDR5 is tethered to chromatin at these genes via an arginine-binding cavity known as the 'WIN' site ([21]), which is the target for WDR5 inhibitors discovered by us ([20–22]) and others ([25–29]). These protein synthesis genes (PSG) are also sites where WDR5 facilitates recruitment of MYC to chromatin ([30]). In MLL1-rearranged (MLLr) leukemia cells, displacement of WDR5 is associated with a reduction in PSG expression, which triggers nu-

cleolar stress and p53-dependent apoptosis ([21]). This effect is not specific to leukemias, as *MYCN*-amplified neuroblastoma (NB) cell lines similarly respond to WIN site inhibition in a p53-dependent manner ([24]). Thus, although the many activities of WDR5 make it difficult to pinpoint a precise mechanism of action of WIN site inhibitors, a recurring theme is their ability to suppress expression of the protein synthesis machinery and to activate p53.

Interestingly, RT cells are sensitive to the FDA-approved translation inhibitor homoharringtonine ([31]) and to the HDM2 inhibitor idasanutlin ([32]), which blocks the ubiquitin-mediated destruction of p53. These two sensitivity profiles align with the characterized response of MLLr cells to WIN site blockade, prompting us to ask whether WIN site inhibitors are active against RT cell lines *in vitro*. We show here that, despite a common genetic lesion, RT cells differ widely in their sensitivity to WIN site blockade, ranging from highly sensitive to functionally nonresponsive. We map the distribution of WDR5 on chromatin in RT cells, show that WDR5 is globally evicted from chromatin by WIN site inhibitor, and define a set of PSGs as direct targets of WIN site inhibitor in this context. Notably, we find that the response of RT cells to WIN site inhibitor does not functionally require p53, and exploit this observation to show that WIN site inhibitors act synergistically with HDM2 inhibitors in this setting, even in RT cells that are weakly sensitive to WIN site inhibition alone. These observations imply that a dual WDR5/HDM2 inhibition strategy could be deployed to one day treat these devastating childhood malignancies.

MATERIALS AND METHODS

Cell culture and transductions

G401, A204, HEK293, MV4:11, and BJ Fibroblasts cells were from ATCC. JMU-RTK-2 and KYM-1 cells were from the JCRB Cell Bank. Aska-SS and HS-SY-II cells were obtained from the RIKEN Cell Bank. TTC642, TTC549, and TM87-16 cells were a gift from Bernard E. Weissman. CHLA-266 and BT-12 cells were gifted from the Children's Oncology Group. G401, JMU-RTK-2, Aska-SS, HS-SY-II, BJ Fibroblasts, and HEK293 cells were maintained in DMEM supplemented with 10% FBS and 1% penicillin/streptomycin. A204, TTC642, KYM-1, TTC549, TM87-16, and MV4:11 cells were maintained in RPMI-1640 supplemented with 10% FBS and 1% penicillin/streptomycin. CHLA-266 and BT-12 cells were maintained in DMEM supplemented with 20% FBS, 1% penicillin/streptomycin, and 1x Insulin-Transferrin-Selenium (ThermoFisher). Viral vector pLKO-p53-shRNA-941 was a gift from Todd Waldman (Addgene plasmid # 25637; http://n2t.net/addgene:25637; RRID:Addgene_25637; ([33])); pLKO-shRNA-scramble was a gift from David Sabatini (Addgene plasmid #1864; http://n2t.net/addgene:1864; RRID:Addgene_1864; ([34]); pXPR_050 was a gift from John Doench and David Root (Addgene plasmids #96925; http://n2t.net/addgene:96925; RRID:Addgene_96925; ([35])); pLX_311-KRAB-dCas9 was a gift from John Doench, David Root, and William Hahn (Addgene plasmid #96918; http://n2t.net/addgene:96918; RRID:Addgene_96918; ([36])). The sgRNA targeting

sequence for *TP53* (CAGGTAGCTGCTGGGCTCCG) was cloned into pXPR_050 via *BsmBI* restriction enzyme (NEB) digestion. To prepare virus, plasmids were transfected into HEK293 cells with psPAX2 packaging (Addgene plasmid #12260; http://n2t.net/addgene:12260; RRID:Addgene_12260) and pMD2.G envelope (Addgene plasmid #12259; http://n2t.net/addgene:12259; RRID:Addgene_12259) plasmids—both gifts from Didier Trono. Transduced cells were selected for six days with 1 µg/mL of puromycin or 10 µg/mL of blasticidin. For shRNA assays, published MV4:11 cells expressing scrambled shRNA or p53 shRNA #941 were used (21).

Proliferation assays

For proliferation assays, cells were plated in 96-well plates and treated with 0.1% DMSO or varying concentrations of C6nc, C6, C16, or Nutlin-3a (Cayman Chemicals) for five days. Cells were quantified using the CellTiter-Glo Luminescent Assay (Promega) according to the manufacturer's instructions. IC_{50} values were calculated using GraphPad Prism software by fitting the data to a normalized-response model. For time course assays, cells were treated with 0.1% DMSO or varying concentrations of C16, and cultures quantified daily for five days with CellTiter-Glo assays. For synergy assays, cells were plated in 384-well plates and treated with a 7×7 matrix of varying concentrations of C16 and Nutlin-3a as well as each compound alone and 0.1% DMSO controls. After five days, cells were quantified by CellTiter-Glo and synergy calculated using the Highest Single Agent Method via the SynergyFinder software (37). Soft-agar assays were performed as described (13,38). Briefly, G401, TTC642, or KYM-1 cells were resuspended in 0.4% agarose-supplemented media with varying concentrations of C16 or 0.1% DMSO control. Cells were added on top of a layer of solidified 0.8% agarose. Fresh C16 or DMSO was added every 2–3 days for a total of 14–21 days. Cells were stained using 0.05% crystal violet in 70% methanol and destained with extensive washing with water. Plates were photographed and colonies counted (blinded) using ImageJ software.

Multiplex gene expression

Cells were treated with 0.1% DMSO or varying concentrations of C16 for 72 hours. To quantify transcripts, a custom QuantiGene™ Plex Assay panel from Thermo Fisher Scientific was used, according the manufacturer's instructions. Probe regions and accession numbers were: *RPS24* (NM_001026, region 5–334)*, RPL35* (NM_007209, region 2–430)*, RPL26* (NM_000987, region 37–445)*, RPS14* (NM_005617, region 61–552)*, RPL32* (NM_000994, region 95–677)*, RPS11* (NM_001015, region 139–634)*, RPL14* (NM_003973, region 108–530)*, GAPDH* (NM_002046, region 2–407) and *HPRT1* (NM_000194, region 102–646). Fluorescence signal was read on a Luminex MAGPIX. Signals from RPGs were normalized to those from *GAPDH* and *HPRT1*, and then to the DMSO control. IC_{50} values were calculated using R package dr4pl (Version 1.1.11; (39)).

Flow cytometry

For cell cycle analysis, 1×10^6 cells were collected after treatment with 0.1% DMSO or C16, fixed in ice-cold 70% ethanol, and stored at -20°C for at least four hours prior to staining. Fixed cells were washed with 1 X phosphate buffered saline (PBS), resuspended in propidium iodide (PI) staining buffer (1X PBS + 10 µg/ml PI + 100 µg/ml RNAse A + 2 mM $MgCl_2$) and stained overnight at 4°C. Cells were filtered through a 35 µm nylon mesh Falcon round bottom test tube and cell cycle distribution quantified using a Becton Dickinson LSRFortessa instrument. For each time point, at least 10,000 cells were counted using forward and side scatter pulse geometry gating to select single cells.

Protein synthesis was measured using the Click-iT Plus OPP Alexa Fluor 488 Protein Synthesis Analysis Kit (ThermoFisher). Cells were treated with either 0.1% DMSO or 500 nM C16 for four days. As a control, a culture of cells were treated with 50 µg/mL of cycloheximide for 30 minutes. Cells were pulsed with 20 µM O-propargyl-puromycin (OPP) for one hour, collected in PBS and fixed with ice-cold 70% ethanol. To control for background, a sample of DMSO- and C16-treated cells were subject to staining without OPP. A Click-iT reaction was then used to conjugate Alexa Fluor488-Azide (1:100 dilution) following the manufacturers instructions. AlexaFluor488 fluorescence was quantified using a BD LSRFortessa instrument. For each sample, 10,000 single cell events were recorded using forward and side scatter pulse geometry gating to select single cells. An unstained control sample was used to identify and exclude autofluorescence in the AlexaFluor488 channel.

The percent of cells progressing through synthesis (S) phase was measured using the FITC BrdU Flow Kit (BD Biosciences). Cells were treated with either 0.1% DMSO or 500 nM C16 for two, four, or seven days then pulsed with BrdU for 30 minutes, collected in PBS, then processed according to the manufacturer's protocol. Briefly, cells were fixed and permeabilized, treated with DNase, incubated with an anti-BrdU antibody conjugated to FITC, and resuspended in 7-AAD solution to stain DNA. FITC and 7-AAD fluorescence were quantified using a BD LSRFortessa instrument. For each sample, 10,000 single cell events were recorded using forward and side scatter pulse geometry gating to select single cells. Unstained control samples were used to identify and exclude autofluorescence.

Western blotting

Cells were washed with PBS and collected in Kischkel Lysis Buffer (150 mM Tris-HCl pH 8.0, 150 mM NaCl, 5 mM EDTA, 1% Triton X-100 with Protease Inhibitor Cocktail (Roche), and PMSF), sonicated, and lysates clarified by centrifugation. Lysates were resolved by SDS-PAGE, transferred to PVDF membrane, and blocked in 5% milk in TBS-T (50 mM Tris, pH 7.5, 150 mM NaCl, 0.1% Tween-20) for one hour. Immunoblotting was performed using the following antibodies: p53 (Santa Cruz sc-126, 1:200), p21 (Cell Signaling #2947, 1:1000), p73 (AbCam ab40658, 1:1000), WDR5 (Cell Signaling #13105, 1:1000), Histone H3–HRP (Cell Signaling #4499, 1:5000),

GAPDH–HRP (Cell Signaling #5174, 1:5000), Cleaved–PARP (Cell Signaling #9541, 1:1000), Goat anti-Rabbit Fc Secondary (ThermoFisher, 1:5000), and Goat anti-Mouse Fc Secondary (Jackson ImmunoResearch, 1:5000). Proteins were visualized using Supersignal West Pico PLUS reagent (Pierce).

Chromatin immunoprecipitations (ChIP)

For each reaction, 1×10^7 cells were treated with 500 nM C16 or 0.1% DMSO for four hours. Chromatin preparation was performed as described (13). Immunoprecipitation was performed using antibodies against WDR5 (Cell Signaling #13105, 5uL per ChIP) or a rabbit IgG control (Cell Signaling #2729). Co-precipitating DNA was quantified using qPCR with published primers (13) against *SNHG15*, *RPS24*, *PUM1*, *RPL35*, *CCT7*, and *METTL1*. ChIP signals were calculated as percent input. For ChIP coupled to next generation sequencing (ChIP-Seq), DNA from three ChIP reactions was pooled and purified using a QIAquick PCR Purification kit (Qiagen). DNA was eluted, size-selected via AMPure XP (Beckman Coulter), and used to generate libraries with the Ultra II DNA library Prep protocol with Multiplex Oligos for Illumina (New England BioLabs). Libraries were sequenced on an Illumina NovaSeq 6000 instrument (150 bp paired-end) by the VANTAGE Core at Vanderbilt University. Three biological replicates for all ChIP-Seq experiments were performed.

RNA-Seq and PRO-Seq

For RNA-Seq, cells were treated with 0.1% DMSO, 500 nM C16, or 500 nM Nutlin-3a for 72 hours. They were collected in Trizol and RNA purified using a Direct-zol RNA Miniprep kit (Zymo Research) following the manufacturer's instructions. After purification, 2 µg of RNA was submitted to the VANTAGE Core who performed ribosomal RNA depletion, library preparation, and sequencing on an Illumina NovaSeq 6000 (150 bp paired-end reads). For PRO-Seq, cells were treated with 0.1% DMSO or 500 nM C16 for two hours, at which point cells were harvested and PRO-Seq reactions performed exactly as described (13,14). PRO-Seq libraries were submitted for sequencing on an Illumina NovaSeq 6000 with 150 paired-end reads by the VANTAGE Core at Vanderbilt University.

Bioinformatics analyses

ChIP-Seq: ChIP-Seq reads were aligned to the human genome hg19 using Bowtie2 (38). Narrow peaks for each sample were called using MACS2 with the options of '-B -q 0.05 -g hs -f BAMPE' (40). Peaks were annotated using Homer (http://homer.ucsd.edu/homer/). Consensus peaks in each condition were identified using DiffBind (http://bioconductor.org/packages/release/bioc/vignettes/DiffBind/inst/doc/DiffBind.pdf) (41). Differential peaks were determined by DESeq2 (42). False Discovery Rate (FDR) < 0.05 was used to identify significantly changed peaks. RNA-Seq: After trimming by Cutadapt (43), RNA-Seq reads were aligned to hg19

using STAR (44) and quantified by featureCounts (45). Differential analysis was performed by DESeq2 (42). FDR < 0.05 was used to identify significantly changed genes. PRO-Seq: Adapters were trimmed and low-quality sequences removed by Cutadapt (43). Reverse complements for reads > 15 bp were generated using FASTX-Toolkit (http://hannonlab.cshl.edu/fastx_toolkit). Reverse-complemented reads were aligned to hg19 using Bowtie2. Reads mapping to rRNA loci and reads with mapping quality < 10 were removed. Reads were normalized by the RLE implemented in DESeq2 (46). Alignment files were used as inputs to NRSA (http://bioinfo.vanderbilt.edu/NRSA/) for estimating alterations of RNA polymerase abundance in proximal-promoter and gene body regions (47). The promoter-proximal region was defined by examining each 50 bp window with a 5 bp sliding step along the coding strand spanning $\pm$ 500 bp from known TSSs; the 50 bp region with the largest number of reads was considered as the promoter-proximal region and its read density was calculated (48). Gene body was defined as the region from +1 kb downstream of a transcription start site (TSS) to its transcription termination site. DESeq2 (42) was implemented to detect significant transcriptional changes for promoter-proximal and gene body regions accounting for the batch effect. Transcriptional changes with an FDR < 0.05 were considered significant.

RESULTS

SMARCB1-deficient cell lines display variable responses to WIN site inhibitor

We profiled early generation WIN site inhibitor C6 and its negative control C6nc (21), as well as chemically-distinct next generation inhibitor C16 (22), against a panel of *SMARCB1*-null cancer cell lines (49–55) (Table 1). We also included in this panel two synovial sarcoma lines in which the presence of an oncogenic SS18-SSX fusion excludes SNF5 from the SWI/SNF complex, triggering SNF5 degradation (56), as well as normal diploid foreskin BJ fibroblasts (57). Most cells in this collection express wild-type p53 (Table 1). Cells were treated for five days with increasing concentrations of compounds and viable cell numbers compared to DMSO controls (Table 1; Figure 1A; Supplementary Figure S1A). Three trends emerged from this analysis. First, the negative control compound C6nc displays little if any activity in these lines. Second, IC_{50} values for C16 are generally lower than those for C6, consistent with its higher affinity for the WIN site (22). The one exception to this is BT-12 cells (Supplementary Figure S1A), where the two inhibitors have comparable potencies (Table 1); likely an indication of off-target activity. And third, these lines exhibit a 100-fold range in sensitivity to WIN site inhibitors. The most sensitive lines—G401 and TTC642—respond almost as well as our benchmark leukemia line MV4;11 (21,22) to both active inhibitors. G401 and TTC642 cells are also sensitive to C16 when assayed in soft-agar for anchorage-independent growth (Supplementary Figure S1B). The least sensitive cells—CHLA-266, Aska-SS, and BJ—in contrast, do not yield measurable IC_{50} values for C6 and give values $\geq$ 9 µM for C16. There is no trend between sensitivity and the different RT types or sites from which the lines were derived.

Table 1. Sensitivity of *SMARCB1*-deficient cell lines to WIN site inhibitors.

| Cell Line	C6nc (μM)	C6 (μM)	C16 (μM)	Tumor Type	Location	Lesion	CCLE *TP53* status	Reference
MV4:11	>25	3.2	0.038 ± 0.009	Leukemia (AML)	Blood (P)	MLL–AF4, FLT3/ITD	no mut	[49]
G401	>25	2.4 ± 0.35	0.098 ± 0.031	MRT	Kidney (P)	SMARCB1 deletion, homozygous	C277F	[55]
TTC642	>25	1.8 ± 0.34	0.138 ± 0.045	MRT	Soft Tissue, Muscle (P)	SMARCB1, nonsense mutation	no mut	[55]
HS-SY-II	>25	2.6 ± 0.61	0.309 ± 0.136	Synovial Sarcoma	Soft Tissue (M)	SS18-SSX1 fusion	no mut	[50]
JMU-RTK-2	>25	16 ± 3.7	0.315 ± 0.075	MRT	Kidney (M)	No SMARCB1 mRNA expression	no mut	[51]
KYM-1	>25	11.2 ± 3.0	0.555 ± 0.098	MRT	Neck (P)	SMARCB1 deletion, homozygous	no mut	[55]
A204	>25	5.9 ± 1.1	0.825 ± 0.187	MRT	Soft Tissue (P)	SMARCB1 deletion, homozygous	no mut	[55]
TTC549	>25	>25	4.5 ± 0.606	MRT	Liver (P)	SMARCB1 deletion, homozygous	no mut	[55]
TM87-16	>25	19.7 ± 9.1	4.6 ± 0.709	MRT	Retroperitoneum, muscle (M)	SMARCB1 deletion, homozygous	no mut	[55]
CHLA-266	>25	>25	7.5 ± 0.525	AT/RT	Brain (P)	SMARCB1 deletion, SMARCB1 mutation	no mut	[54]
Aska-SS	>25	>25	10.4 ± 1.1	Synovial Sarcoma	Soft Tissue (P)	SS18-SSX1 fusion	unreported	[52]
BT-12	>25	6.8 ± 1.1	11 ± 3.3	AT/RT	Brain (P)	SMARCB1 deletion, homozygous	no mut*	[52]
BJ	>25	>25	8.7 ± 1.40	Normal diploid fibroblasts	Foreskin	None	NA	[57]

Cell lines were treated with seven-point serial dilution set of compounds for five days, and cell numbers determined by CellTiter-Glo. Cell numbers for each dose were normalized to those from DMSO-treated samples and used to calculate mean IC_{50} values, which are shown along with SEM ($n \geq 3$). >25 indicates that the top concentration of compound used (25 μM) did not reduce cell number below 50%. (P) or (M) in Location column indicates if cell line was derived from the primary tumor (P) or a metastatic (M) site. Lesion indicates relevant mutation or *SMARCB1* expression status. Note that CHLA-266 cells have two distinct lesions in *SMARCB1*. *TP53* mutational status is taken from the Cancer Cell Line Encyclopedia ([53]). 'no mut' indicates no *TP53* mutation reported in that line. *Note that BT-12 cells do not express mutant p53, but have an impaired p53 response, likely due to deletion of CDKN2A ([32]).

From these data we conclude that, although all RT lines display sensitivity to WIN site inhibitors, the response within this set of cancer cells—connected by a common oncogenic lesion—varies by up to two orders of magnitude.

It is possible that the differential response of these cells to WIN site inhibitors stems from differences in intracellular compound levels or activity in each line. We reasoned that we could determine the efficiency with which WIN site inhibitors engage WDR5 in cells by quantifying their effects on expression of a set of direct WDR5 target genes. We developed a WDR5 target engagement assay that uses QuantiGene™ Plex technology to assess transcript levels from seven RPGs, five of which (*RPS14, RPS24, RPL26, RPL32,* and *RPL35*) are universally bound by WDR5 and suppressed by WIN site inhibitor ([21,24]) and two of which (*RPS11* and *RPL14*) are never bound and are unresponsive to WIN site blockade. As expected ([21,24]), WDR5-bound RPGs are suppressed by a factor of two in all lines examined (Figure 1B), while the non-WDR5-bound RPGs do not change or are modestly induced. By performing dose-response analyses, we calculated IC_{50} values for RPG suppression in a representative sample of RT lines (Figure 1C and Supplementary Figure S1C), as well as MV4:11 and BJ cells. In most cases, IC_{50} values for RPG suppression are double digit nanomolar, and close to the cellular IC_{50} values for the more sensitive RT cell lines. There are differences in the efficiency with which each of the RPGs are

suppressed by C16 in each line, but these differences are generally within a factor of three, and do not correlate with cellular growth response. Thus, although cellular context can impact the efficiency with which WIN site inhibitors act, differences in the ability of compounds to inhibit WDR5 cannot explain the differential cellular sensitivities we observe.

Finally, we characterized how growth of two of the most sensitive RT lines, G401 and TTC642, is impacted by WIN site inhibition. Over the course of a five day treatment, C16 induces a dose-dependent and progressive decrease in cell numbers compared to the DMSO control (Supplementary Figure S1D). At all dose levels, absolute cell numbers at the end of treatment are higher than at the beginning, consistent with a reduction in expansion, rather than a cell death response (Supplementary Figure S1E). Treating cells with 500 nM C16—a concentration sufficient to maximally inhibit RPG transcripts in all lines (Figure 1C)—we observe only modest changes in cell cycle phase distribution (Supplementary Figure S1F), and pulse-labeling with BrdU reveals that, although DNA synthesis is decreased by C16, a significant percentage of cells (∼15%) are still progressing through S-phase after two, four, and seven days of treatment (Supplementary Figure S1G). Taken together, these data reveal that the primary mode of response of sensitive RT lines to WIN site inhibition is a reduction in the rate of proliferation, rather than cell cycle arrest or cell death.
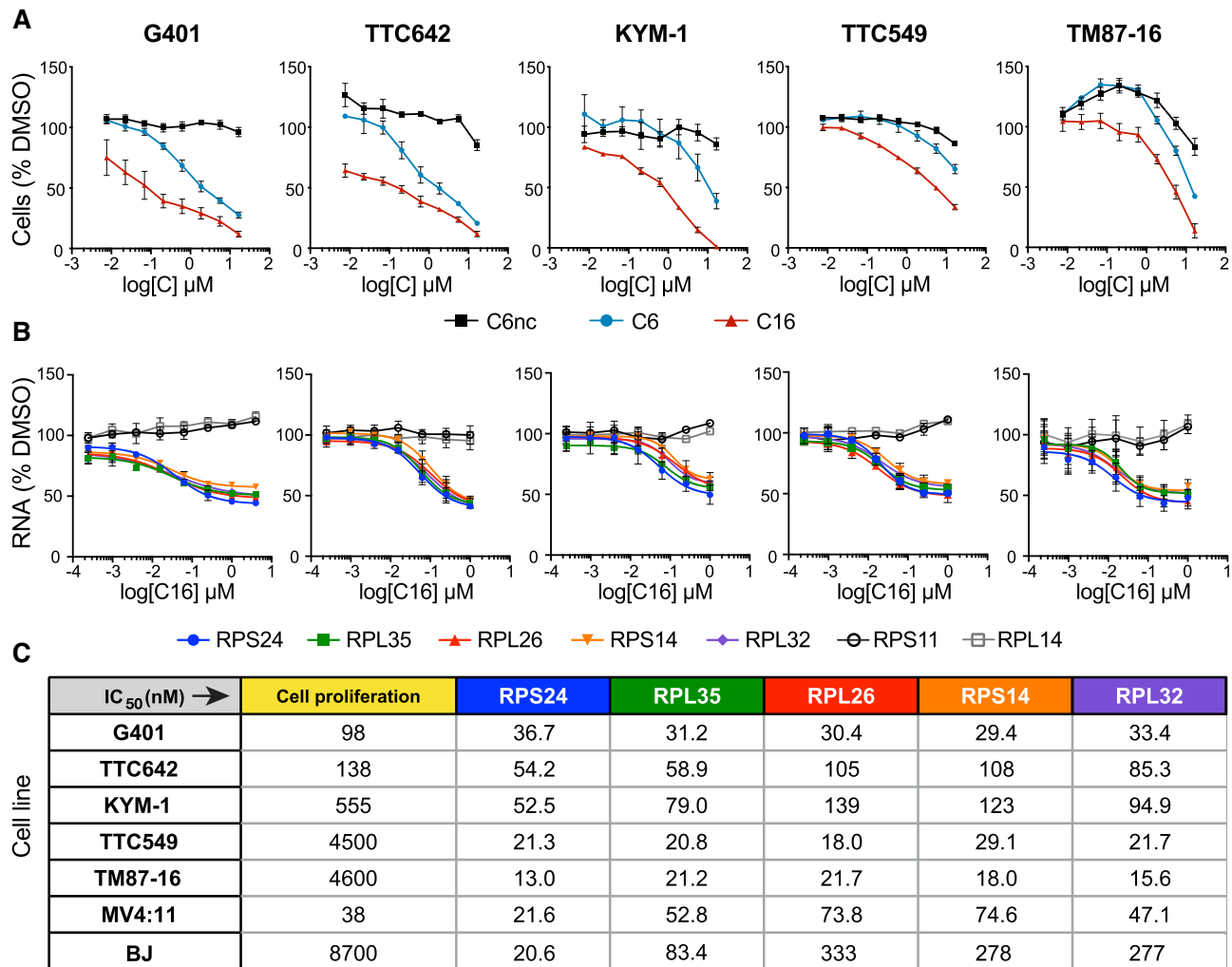
Figure 1. WIN site inhibitors are active against *SMARCB1*-deficient cell lines. (**A**) Dose response of indicated lines to C6nc, C6, or C16 in a five day treatment. Data are expressed as the percentage of cells remaining at day five, compared to the DMSO control ($n = 3$, mean SEM). (**B**) Cell lines were treated for three days with increasing concentrations of C16, and RNA levels for RPGs determined via Quantigene^{TM} arrays. RNA signal is expressed as a percentage of the equivalent DMSO control for each RPG in each line, normalized to *GAPDH* and *HPRT1*. RPGs with colored lines bind WDR5 and are suppressed two-fold by WIN site inhibitor; those in black and gray are unbound and not suppressed ($n = 3$, mean $\pm$ SEM). (**C**) Summary of IC$_{50}$ values obtained for C16 in cell proliferation (A) and RPG (B) expression in the indicated cell lines. SEM for the cell proliferation IC$_{50}$ values are listed in Table 1; 95% confidence intervals for IC$_{50}$ values for RPG expression are in Supplemental Figure S1C.

WIN site inhibitor displaces WDR5 from chromatin in RT cells

Next, we used chromatin-immunoprecipitation coupled to next generation sequencing (ChIP-Seq) to track the location of WDR5 on chromatin in two RT lines, G401 and KYM-1. Consistent with studies in other cell lines (21,24,30), there is a considerable difference in the number of WDR5 binding sites in the two RT lines, ranging from ~160 in G401 to ~700 in KYM-1 cells (Figure 2A; Supplementary Table S1). As with earlier studies, binding sites for WDR5 in these RT lines are predominantly promoter proximal, with a majority occurring within 1 kb of an annotated transcriptional start site ('TSS'; Figure 2B). Assigning all genes within 2 kb upstream of an annotated TSS, or anywhere within a transcription unit, links these binding sites to ~148 genes for G401, and ~649 genes for KYM-1, cells which, by gene ontology (GO) enrichment analysis, cluster strongly

in terms related to protein synthesis (Figure 2C). This set includes half of the RPGs (Supplementary Figure S2A), most of which are bound by WDR5 in all cell lines examined. Comparing these binding events with our previously-defined 'universal' set of ~100 human WDR5 binding sites (24), we observe that almost all the universal sites are found in both RT lines (Figure 2D), extending the presence of these near-ubiquitous binding sites to the rhabdoid tumor context. From this analysis, we conclude that the pattern of WDR5 localization on chromatin in RT cells matches expectations from other cell lines in terms of both the location of WDR5 binding and the nature of genes bound.

To determine if the integrity of the WIN site is required to tether WDR5 to chromatin in G401 and KYM-1 cells, we treated them for four hours with 500 nM C16; a concentration that maximally inhibits RPG transcript levels in both lines (Figure 1B). Under these conditions, C16 results in
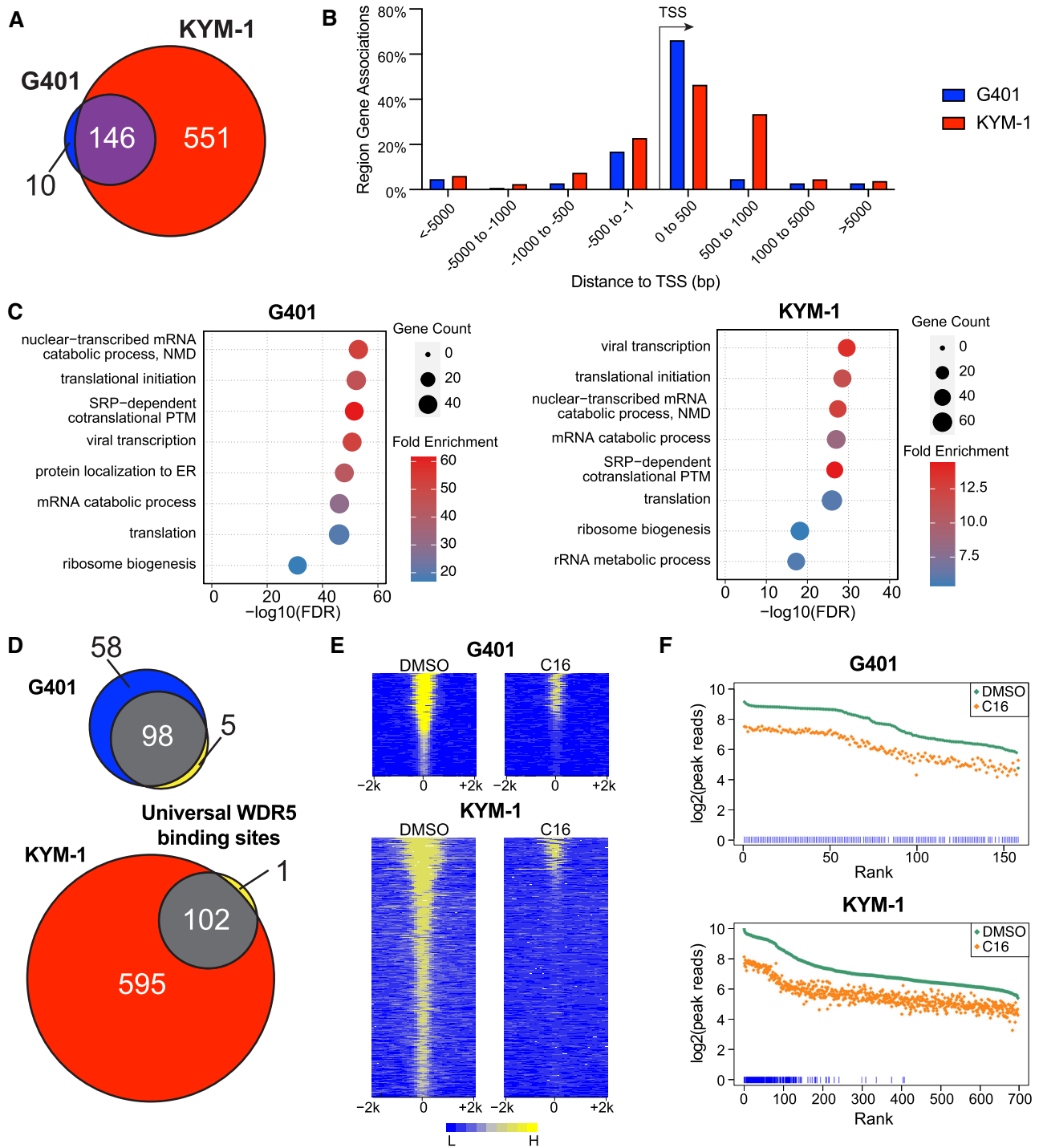
Figure 2. WIN site inhibitor displaces WDR5 from chromatin in RT cells. (**A**) Venn diagram, showing the overlap of WDR5 peaks in ChIP-Seq data from G401 and KYM-1 cells. Data are from DMSO control samples of the experiment presented in (E–F) (*n* = 3). (**B**) Distribution of WDR5 binding sites in G401 and KYM-1 cells, binned according to distance from the closest annotated transcriptional start site (TSS). (**C**) GO term enrichment analysis of WDR5-bound genes, defined as those in which a WDR5 binding site is located within 2 kb of an annotated TSS or within a transcription unit. Biological Process GO terms were ranked by false discovery rate (FDR). The eight most significantly enriched terms are shown. Color indicates fold enrichment, size indicates gene number, and the x-axis is the -$\log_{10}$(FDR). (**D**) Venn diagrams, showing the overlap of WDR5 peaks detected in G401 and KYM-1 cells with the set of 103 'universal' human WDR5 binding sites (24). (**E**) Heatmaps of WDR5 ChIP-Seq peak intensity in G401 or KYM-1 cells treated for four hours with DMSO or 500 nM C16. Images represent the combined average of normalized peak intensity in 100-bp bins ± 2 kb around the center of peaks. Peaks are ranked based on DMSO-treated samples for each cell line. (**F**) Ranking of WDR5 peak intensities in G401 or KYM-1 cells treated with DMSO (green) or 500 nM C16 (orange). Peaks are ranked according to peak reads in DMSO samples and expressed as log2 values for clarity. Blue lines at the bottom of each graph indicate the common WDR5 binding sites shared in G401, KYM-1, and TTC549 cells.

the global reduction of WDR5 association with chromatin (Figure 2E–F; Supplementary Figure S2B), as measured by ChIP-Seq. We confirmed this result by gene-specific ChIP-qPCR in both lines (Supplementary Figure S2C). The nature of the effect is similar to what we reported with C6 in leukemia cells (21,24), both in terms of the magnitude of reduction in WDR5 binding, as well as the fact that WDR5 is displaced from both shared and cell-type specific WDR5 binding sites by C16 (Figure 2F; Supplementary Figure S2B). Taken together with other studies, these data support the notion that the WIN site globally tethers WDR5 to chromatin, and reveal that WIN site inhibitors have a consistent, cell-type independent, ability to comprehensively evict WDR5 from its chromatin locations.

Lastly, we asked whether these key observations made in sensitive RT cell lines—binding of WDR5 to chromatin at conserved protein synthesis genes and displacement of WDR5 from chromatin by C16—apply to a relatively insensitive RT line, TTC549 (Supplementary Table S1). WDR5 binding sites in TTC549 cells overlap extensively with those in G401 and KYM-1 cells (Supplementary Figure S2D), show a similar pattern of promoter-proximity (Supplementary Figure S2E), cluster in genes connected to protein synthesis (Supplementary Figure S2F), and encompass almost all of the universal WDR5 binding sites (Supplementary Figure S2G), including the specific subset of RPGs (Supplementary Figure S2A). Importantly, 500 nM C16 treatment is sufficient to evict WDR5 from chromatin genome-wide in TTC549 cells (Supplementary Figure S2H–J). There is thus no substantive difference in the localization of WDR5 on chromatin, nor the effects of C16, in an insensitive RT line that can explain the lack of an overt cellular response to WIN site blockade. We conclude that differences in the way RT cells respond to WIN site inhibitor are likely a consequence of downstream cellular characteristics, rather than those related to the actions of WDR5 on chromatin or the primary response to WIN site inhibition.

WDR5-bound protein synthesis genes are early transcriptional targets of WIN site inhibitor

To identify direct transcriptional targets of WIN site inhibitor in G401 and KYM-1 cells, we used PRO-Seq (58), a global nuclear run-on, to ask how the distribution of active RNA polymerases is altered after two hours of exposure to C16. This analysis (Figure 3A; Supplementary Figure S3A; Supplementary Table S2) revealed a small set of transcriptional changes in both lines, as measured by differences in gene body associated active RNA polymerases. Genes with increased transcription are dissimilar; there is no overlap between induced genes between G401 and KYM-1 cells (Figure 3B), and none of the genes bound by WDR5 are induced by WIN site blockade in the same line (Supplementary Figure S3B). Genes with decreased transcription, in contrast, are almost identical between the two lines (Figure 3B), and are enriched in those bound by WDR5, as determined by manual inspection (Figure 3C) and gene set enrichment analysis (GSEA; Figure 3D). As expected, GO analysis reveals enrichment in genes connected to protein synthesis (Supplementary Figure S3C), including a recurring set of RPGs (Supplementary Figure S3D), as well as genes encod-

ing the nucleolar RNAs SNHG15 and SNHG17, the cell cycle transcription factor E2F3, translation initiation factors EIF4G3, EIF4G1, and EIF3D, and the translation elongation factor EEF1G (Figure 3C).

Because of the importance of enhancer dysregulation in RT (8,9), we used the Nascent RNA Sequencing Analysis (NRSA) pipeline (59) to mine these PRO-Seq data for the presence of active enhancers in G401 and KYM-1 cells, detected by the presence of divergent transcription at gene distal sites (Supplementary Figure S3E and Supplementary Table S3). By these criteria, active enhancers in the two cell lines are disparate (Figure 3E), consistent with previous reports that different rhabdoid tumors have unique enhancer landscapes (8). Notably, WIN site inhibition has only modest effects on enhancer function in either cell line (Figure 3F). Moreover, using published H3K27 acetylation data from G401 cells (8) to distinguish between superenhancers (SE) and traditional enhancers (TE) in this line (Supplementary Figure S3F), we observe that genes with changes in the distribution of active RNA polymerases with C16 have little if any enhancer connections (Figure 3G), again consistent with the idea that WIN site blockade does not appreciably alter enhancer status in these two RT lines.

Four important conclusions can be drawn from these results. First, in both cell types, a majority of genes bound by WDR5 do not rapidly respond transcriptionally to WIN site inhibition, even though WDR5 is displaced from chromatin at these genes. Second, the impact of WIN site inhibitor on gene transcription is small, both in terms of the number of genes involved and the magnitude of the response. Third, enhancer function is not appreciably nor consistently altered by WIN site inhibition in these cells. And fourth, the predominant transcriptional response to WIN site inhibitor in RT cells is inhibition of transcription at WDR5-bound genes, a majority which are linked to protein synthesis. We conclude that, as in other cell types (21,24) these PSGs are the primary transcriptional targets of WIN site inhibitor in RT cells.

WIN site inhibitor induces p53 target genes in SMARCB1-deficient cells

To expose transcriptomic changes induced by C16 in RT cells, we performed RNA-Seq in five SMARCB1-deficient cell lines treated for three days with C16. Three more sensitive (G401, TTC642, and KYM-1) and two less sensitive (TTC549 and TM87-16) lines were profiled. This analysis (Figure 4A; Supplementary Figure S4A–B) identified between ~1,700 and ~5,700 differentially expressed genes, depending on the cell type. In general, the response of the more sensitive lines is greater than that of the less sensitive, both in terms of the number of genes (Figure 4A) and the magnitude of changes (Figure 4B). Across all lines, we observe that between one quarter and two thirds of the differentially expressed genes are cell type-specific (Supplementary Figure S4C), illustrating the diversity of the transcriptional response to C16 within this panel. Principal component analysis (PCA) reveals that this diversity is likely a consequence of the diverse native transcriptomes of the five lines, rather than disparate responses to C16 (Supplementary Figure S4D). Contrasting the more sensitive with
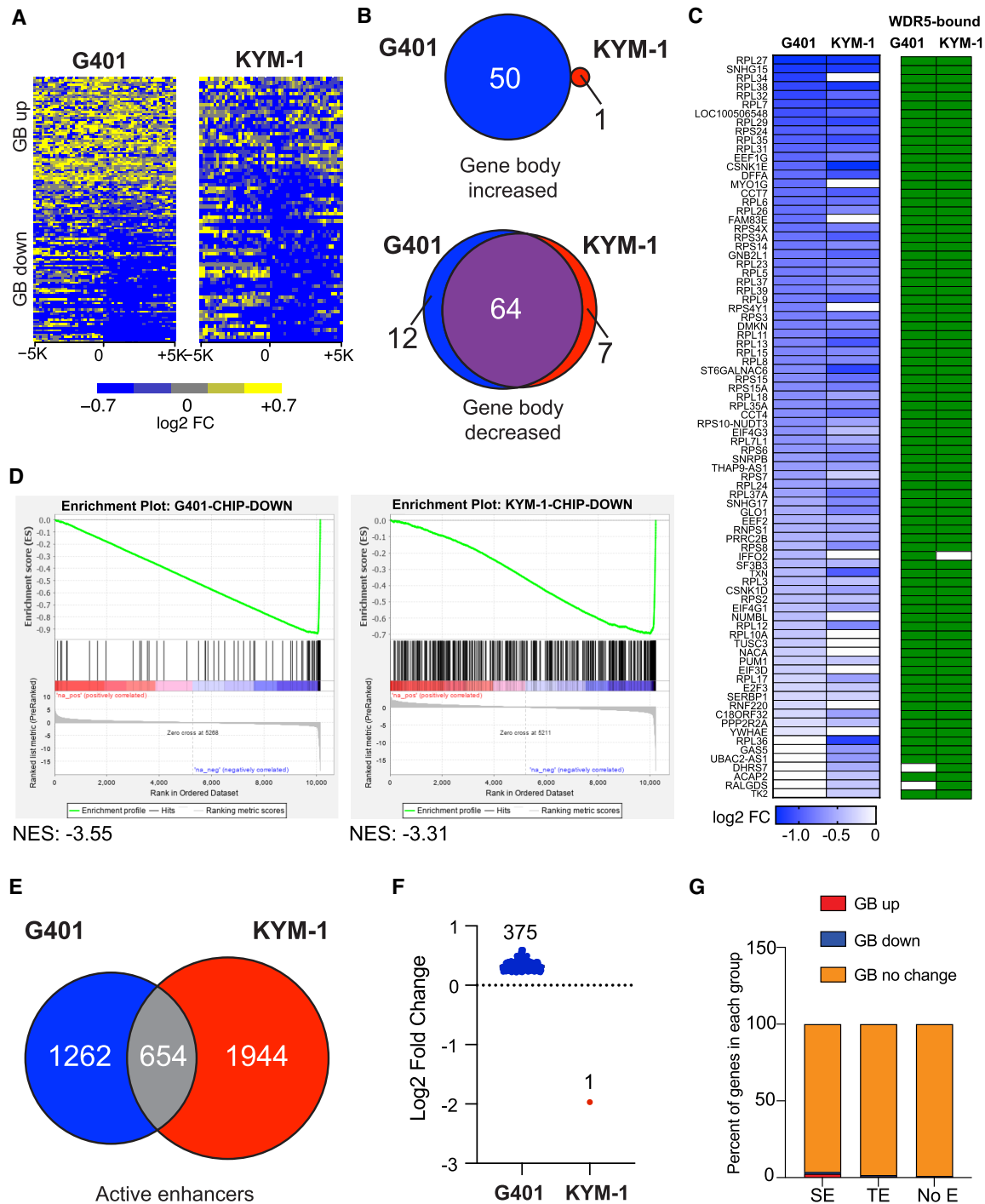
Figure 3. WDR5-bound protein synthesis genes are direct targets of WIN site inhibitor in RT cells. (**A**) Heatmap, displaying log$_2$-fold (log2 FC) change of active polymerases in G401 or KYM-1 cells treated for two hours with 500 nM C16, compared to their respective DMSO controls, as determined by PRO-Seq. Maps are ranked individually within each cell type, and show changes in polymerase density in the promoter-proximal region and +/- 5 kb around the TSS (200 bp bins). The top of the figure shows genes where transcription in the gene body (GB) increased (GB up); the lower part shows genes where gene body transcription decreased (GB down) (*n* = 2). (**B**) Venn diagrams, comparing genes showing an increase or decrease in gene body associated polymerases in response to C16 in G401 versus KYM-1 cells. (**C**) Heatmap (*left*), showing genes with significant decreases in gene body-associated polymerases in G401 or KYM-1 cells treated with 500 nM C16. The green bars to the right indicate if WDR5 is bound to that locus in each cell type (ChIP-Seq). *LOC100506548* is read-through transcription from *RPL37*. (**D**) Gene set enrichment analysis (GSEA) comparing genes with a reduction in WDR5 binding by ChIP-Seq against a gene list ranked by alteration in the density of gene body-associated transcribing polymerases in C16-treated G401 and KYM-1 cells. FDR q = 0.0 in both cases. (**E**) Venn diagram, showing overlap of active enhancers in G401 and KYM-1 cells, as determined by PRO-Seq. (**F**) Plot showing the number and magnitude (log2 fold-change) of enhancer activity changes elicited by C16 treatment of G401 and KYM-1 cells. (**G**) Graph showing the percentage of genes with a C16-induced change in gene body (gb) associated RNA polymerases, binned according to whether they are proximal to a superenhancer (SE), traditional enhancer (TE), or no enhancer (No E). Enhancer status was called by ranking H3K27ac-positive, H3K4me3-negative, peaks from (8) according to H3K27ac signal, as show in Supplementary Figure S3F.
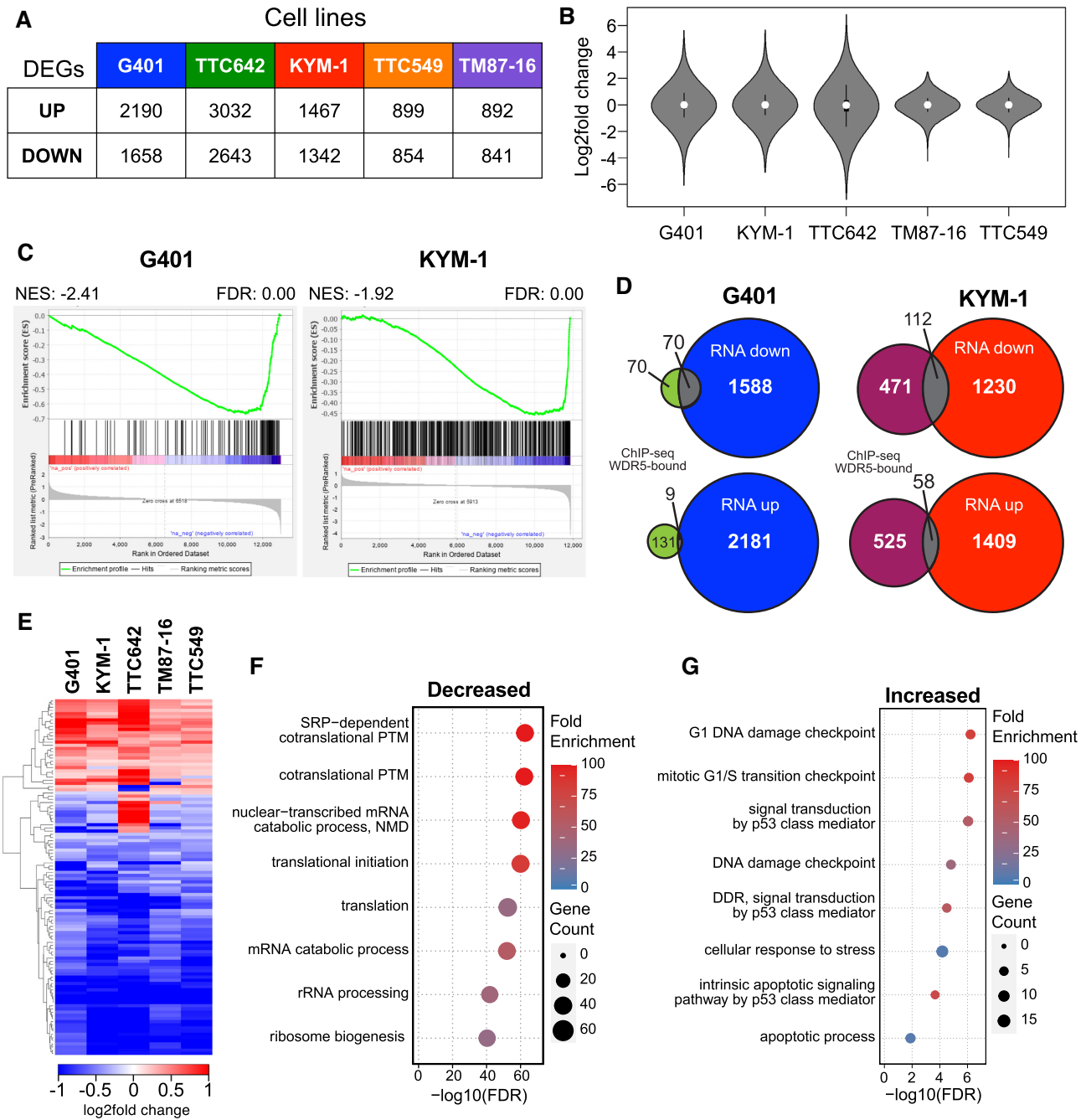
Figure 4. C16 suppresses WDR5-bound PSGs and induces p53 target genes in RT cells. (**A**) Table shows the number of differentially expressed genes (DEGs; FDR < 0.05) altered by three days of treatment of the indicated cell lines with 500 nM C16, compared to respective DMSO controls ($n = 2$ for G401, TTC642, and KYM-1 cells; $n = 3$ for TTC549 and TM87-16 cells). (**B**) Violin plot, showing the distribution of $\log_2$-fold transcript changes elicited by C16 (RNA-Seq) in each line. (**C**) GSEA, comparing genes bound by WDR5 in ChIP-seq against a gene list ranked by alteration in expression, as determined by RNA-Seq. G401 cell data is on the left, KYM-1 cell data is on the right. 'NES'; normalized enrichment score. 'FDR'; false discovery rate. (**D**) Venn diagram, showing the overlap of genes bound by WDR5 in G401 and KYM-1 cells (ChIP-Seq) with those that are suppressed ('RNA down') or induced ('RNA up') by three days of C16 treatment. (**E**) Heatmap showing the $\log_2$FC of significantly (FDR < 0.05) changed transcripts that are altered by C16 in all five cell lines. Transcripts are clustered according to the relationship in expression changes between the cell lines. (**F**) GO term enrichment analysis of genes showing a significant decrease in expression in all five lines, as determined by RNA-Seq. Biological Process GO terms were ranked by false discovery rate (FDR). The eight most significantly enriched terms are shown. Color indicates fold enrichment, size indicates gene number, and the x-axis is the -log10(FDR). (**G**) As in (F) but for common genes with increased expression.

the less sensitive lines, the 67 genes with decreased expression only in the more sensitive cells (Supplementary Figure S4C) fail to cluster into any biological category. There are 81 genes induced only in more sensitive cells, including a small but highly enriched set encoding mitochondrial respiratory chain complex I (Supplementary Figure S4E). Looking at G401 and KYM-1 cells, where we have both binding data for WDR5 (Figure 2) and early transcriptional responses (Figure 3), there is a tendency of WDR5-bound genes to be persistently suppressed by C16 (Figure 4C and D), and a majority of genes with decreased transcription by PRO-Seq are decreased in RNA-Seq (Supplementary Figure S4F). Notably, however, most genes with altered expression in RNA-Seq are neither bound by WDR5 nor respond early (Figure 4D and Supplementary Figure S4F), indicating that the predominant long term transcriptional response to C16 in these cells is likely a secondary consequence of WIN site blockade, rather than differences in primary transcriptional effects.

Just 90 genes are differentially expressed in response to C16 in all lines (Supplementary Figure S4C), the majority of which change in the same direction and within a factor of two (Figure 4E). An exception to this trend is a group of ten genes induced in TTC642 but suppressed in all other lines, most of which encode variants of histone H2A and H2B. GO analysis of the ~70 genes with decreased transcription in all lines reveals strong enrichment in terms connected to protein synthesis (Figure 4F), including the recurrent set of 38 RPGs (Supplementary Figure S4G) and a handful of translation factors (Supplementary Table S4). Only 23 genes are induced in all lines (Supplementary Table S4), and although this set is small it is significantly enriched in genes linked to p53 signaling (Figure 4G). Indeed, curation of this list reveals that 16 of these genes are induced by p53 (Supplementary Table S4), including *ZMAT3* (60), *CDKN1A* (p21), and *CCND1* (Cyclin D1). Connections to p53 are further reinforced by results of Reactome Pathway analysis (61) which captures significant enrichment in all lines for 'Transcriptional Regulation by p53' (Supplementary Figure S4H) and by GSEA (Supplementary Table S5) which returned positive enrichment in 'Hallmark p53 pathway' in all RNA-Seq datasets except for KYM-1 cells (Supplementary Figure S4I). Based on these analyses, we conclude that WDR5-bound PSGs are early and persistent targets of WIN site inhibitor in RT cells. We also conclude that activation of p53 target genes is a recurring response to WIN site inhibition in this panel.
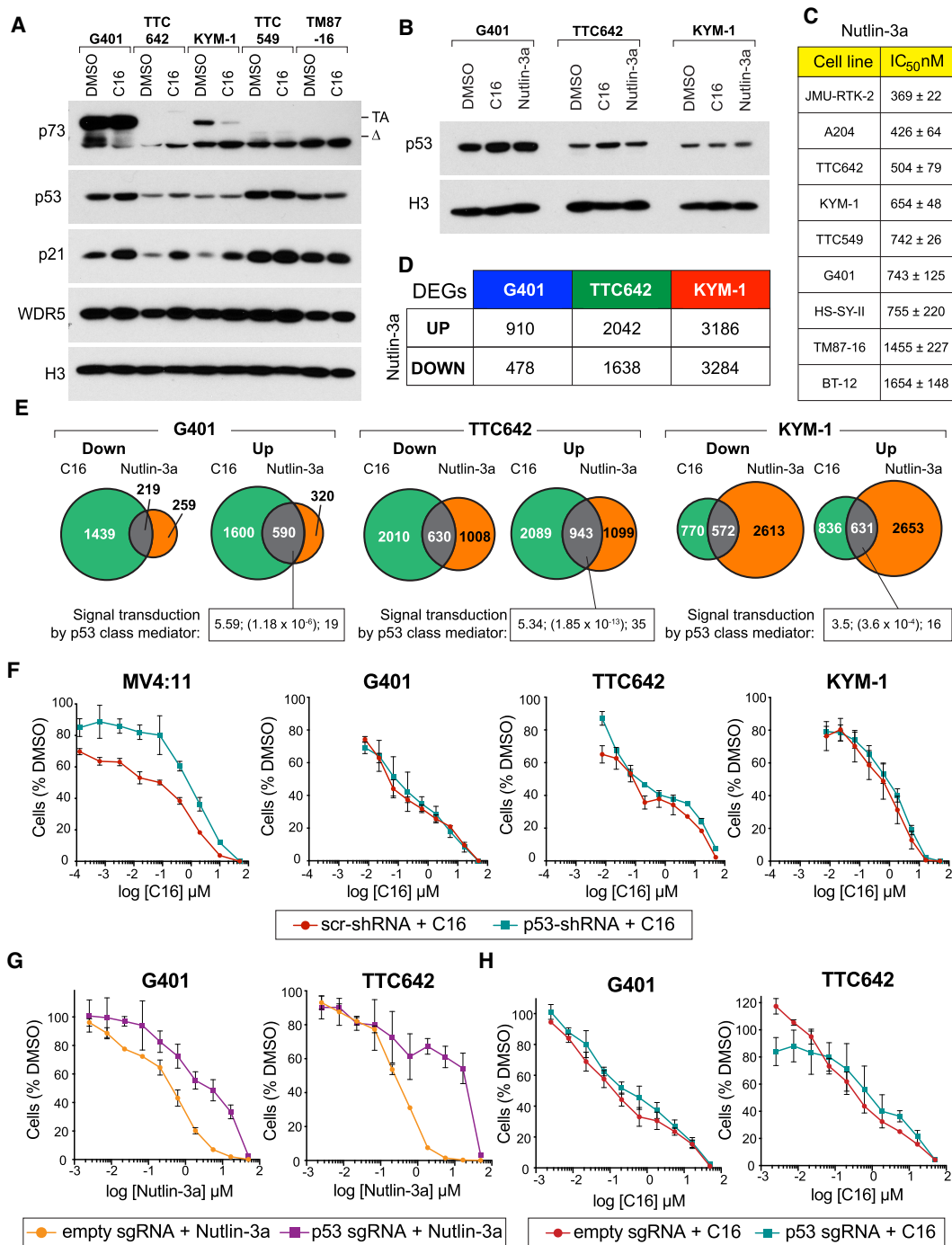
The response of SMARCB1-deficient cells to WIN site inhibitor is p53-independent

The transcriptional response of RT lines to C16 mirrors what we reported with WIN site inhibitors in MLLr (21) and NB (24) cells; suppression of WDR5-bound RPGs and activation of p53 target genes. We also observe a similar ~20% reduction in protein synthesis capacity (Supplementary Figure S5A), as measured by pulse-labeling with O-propargyl-puromycin (OPP) (62). We therefore asked whether, as in these other cells, p53 is induced by C16 in RT cells. Curiously, we observe subtle induction of p53 protein in G401 and TTC642 cells, but not in three other RT lines

profiled (Figure 5A). By RNA-Seq, none of these lines express the p53 family member p63, and the transcriptionally-active isoform of p73, TAp73, is either not expressed, unchanged, or decreased by C16 treatment (Figure 5A). Thus, despite the modest activation of p53 target genes detected in our C16 RNA-Seq experiments, induction of p53 itself is not recurringly detected at the protein level in this panel.

It is possible that induction of p53 by C16 is too small to detect by Western blotting, as opposed to the more sensitive output provided by p53 target gene expression. To test if p53 target gene activation can be measured in the absence of robust changes in p53 protein, we treated G401, TTC642, and KYM-1 cells with the HDM2 antagonist Nutlin-3a (63) at 500 nM for three days—a dosage that fails to induce detectable changes in p53 protein levels (Figure 5B), but is close to the IC_{50} for cellular proliferation for each line (Figure 5C). Under these conditions, RNA–Seq (Supplementary Figure S5B–C) tracks between ~1,400 and ~6,500 differentially expressed genes, depending on cell type (Figure 5D). As we observed with WIN site inhibitor, the magnitude of the response is modest (Supplementary Figure S5D) and the deregulated genes are disparate across the three lines (Supplementary Figure S5E). GO analysis of the 49 commonly suppressed genes revealed modest enrichment in categories related to amino acid metabolism (Supplementary Figure S5F), whereas analysis of the 206 commonly induced genes returns strong and significant enrichments in terms related to induction of p53 (Supplementary Figure S5G). These connections to p53 are further reinforced by results of GSEA (Supplementary Table S6), which reports significant enrichment in hallmark p53 target genes in each of the lines (Supplementary Figure S5H). Overlaying the Nutlin-3a RNA-Seq with that of the C16 in each line reveals a high degree of similarity between the transcriptional responses to both treatments and, as expected, the overlap in each line for induced genes coalesces on targets of p53 (Figure 5E). Together, these data reinforce the concept that p53 target genes are induced by C16 in RT cells. At the same time, because induction of p53 is evidenced only by target gene expression changes, and not at the level of p53 protein, these data also support the idea that induction of p53 by WIN site inhibitor is relatively subtle.

Given the subtle induction of p53 we observed, we next asked if p53 is required for the overt cellular response of RT cells to WIN site inhibitor, as it is in MLLr (21) and NB (24) cell lines. We attenuated p53 expression with a previously published shRNA (21) in G401, TTC642, and KYM-1 cells, and confirmed p53 knockdown by Western blotting (Supplementary Figure S5I). We also performed RNA-Seq on G401 cells expressing the p53 (or scrambled control) shRNA, with and without C16 treatment (Supplementary Figure S5J–K). Notably, the GO term 'signal transduction by p53' is only observed in the C16-treated scramble shRNA control cells—not in treated cells expressing the shRNA against p53 (Supplementary Figure S5L); the same applies to enrichment of hallmark p53 target genes, as determined by GSEA (Supplementary Table S7). And of the 35 consensus p53 target genes (64) altered by C16 treatment in G401 scrambled shRNA control cells, 33 are either not altered, or altered to a lesser extent, by C16 in p53 shRNA knockdown cells (Supplementary Figure S5M). Together,

Figure 5. Growth response of *SMARCB1*-deficient cells to WIN site inhibitor is p53-independent. (**A**) Western blot, performed on lysates from the indicated lines that were treated with DMSO or 500 nM C16 for three days. For p73, isoforms carrying the transcriptional activation domain (TA), or lacking this domain (Δ), are visible. Histone H3 is a loading control. Image is representative of three biological replicates. (**B**) Western blot, performed on lysates from the indicated cell lines that were treated with DMSO, 500 nM C16, or 500 nM Nutlin-3a for three days. Image is representative of three biological replicates. (**C**) Table shows the IC$_{50}$ values for Nutlin-3a in each cell line, calculated by performing a dose-response analysis in a five day treatment. The IC$_{50}$ column shows the IC$_{50}$ values $\pm$ SEM ($n = 3$). (**D**) Table shows the number of transcripts significantly (FDR < 0.05) altered by three days of treatment of cell lines with 500 nM Nutlin-3a, compared to respective DMSO controls, as determined by RNA-Seq. 'DEGs'; differentially expressed genes ($n = 3$). (**E**) Venn diagrams, showing the overlap of significantly differentially expressed genes ('Down'–decreased; 'Up'–increased) in response to C16 or Nutlin-3a treatment in each line. For common induced genes, the fold enrichment, (FDR), and number of genes for the GO Biological Process term 'Signal Transduction by p53 class mediator' are shown in the box below, separated by semi-colons. (**F**) Dose response of the indicated cell lines, stably expressing either a scrambled shRNA ('scr-shRNA') or an shRNA against p53 ('p53-shRNA'), to C16. Five day assay. Data are expressed as the percentage of cells remaining at day five, compared to the DMSO control ($n = 3$, mean $\pm$ SEM). (**G**) Dose response of the indicated cell lines, stably transduced with a vector expressing inactive Cas9 fused to the KRAB repressor domain, as well as either an 'empty' vector or a vector expressing a single guide RNA (sgRNA) against p53, to Nutlin-3a. Five day assay. Data are expressed as the percentage of cells remaining at day five, compared to the DMSO control ($n = 3$, mean $\pm$ SEM). (**H**) As in (G), except cells were treated for five days with C16 ($n = 3$, mean $\pm$ SEM).

these data demonstrate that the p53 shRNA used in this instance is capable of both physically and functionally suppressing p53.

As expected (21), shRNA-mediated knockdown of p53 results in a significant rightward shift in the response of MV4:11 cells to C16, increasing the IC_{50} from 40 nM to 750 nM (Figure 5F). Using the same shRNA against p53, however, we see little if any impact on the dose-response curves of G401, TTC642, and KYM-1 cells to C16 treatment (Figure 5F). To confirm the dispensability of p53 in the RT cell response to WIN site blockade, we independently knocked down p53 expression using an orthologous CRISPRi-based approach (35,36) in G401 and TTC642 cells. Here, we observed robust suppression of p53 levels (Supplementary Figure S5O), and the expected rightward shift in Nutlin-3a sensitivity curves (Figure 5G), but again there is little if any change in the response of these cells to WIN site inhibitor C16 (Figure 5H). Thus, despite a common activation of p53 target genes in RT cell lines, and a strong expectation that the cellular response to C16 is mediated via p53, the growth response of these *SMARCB1*-deficient cell lines respond to WIN site inhibitor is p53-independent.

C16 and Nutlin-3a synergistically inhibit RT cell proliferation

Because *SMARCB1*-deficient cells are sensitive to both WDR5 and HDM2 inhibition, and because the growth response of these cells to WDR5 inhibition is independent of p53, we reasoned that C16 and Nutlin-3a should act synergistically in this setting. We performed five-day cell proliferation assays with C16 and Nutlin-3a dose combinations, along with corresponding single-agent treatments, with our two most sensitive (G401 and TTC642) and two least sensitive (TTC549 and TM87-16) RT lines. Cell viability following each treatment was normalized to DMSO treatment and synergy scores for each combination were calculated utilizing the highest single agent (HSA) model (65).

As monitored by both average and peak synergy scores, we observe synergy between C16 and Nutlin-3a in all four lines (Figure 6A and Supplementary Figure S6A). The greatest synergy is seen in TTC642 cells, which we classify as sensitive to C16 alone, but less sensitive lines TTC549 and TM87-16 also display synergy across a broad range of C16 and Nutlin-3a concentrations. Importantly, synergy is also apparent in G401 and TTC549 cells with a second, chemically-distinct, HDM2 inhibitor HDM201 (66) (Supplementary Figure S6B–C), and is reduced by either shRNA- (Supplementary Figure S6D–E) or CRISPRi- (Supplementary Figure S6F–G) mediated knockdown of p53, demonstrating that synergy is mediated via an on-target activity of Nutlin-3a against HDM2.

The simplest explanation for the synergy we observe is that the combination of WIN site inhibitor and HDM2 antagonist yields a more pronounced activation of p53—and p53 target genes—than either agent alone. Indeed, this is what we observe. Co-treatment of RT lines with 500 nM each of C16 and Nutlin-3a results in a stronger induction of p53 then either individual treatment (Figure 6B), and leads to enhanced activation of the canonical p53 target

p21, as measured by Western blotting (Figure 6B). Further analysis of consensus p53 target genes by reverse-transcriptase Q-PCR revealed similar synergistic induction of p21 (*CDKN1A*), *HDM2*, *TP53INP1*, and *BTG2* in TTC549 (Figure 6C) and G401 and TTC642 cells (Supplementary Figure S6H). Suppression of WDR5-bound RPGs *RPL35* and *RPS24* by C16, in contrast, was not further enhanced by the addition of Nutlin-3a (Figure 6C and Supplementary Figure S6H). Based on these data, we conclude that—independent of the magnitude of response of RT cells to C16 alone—WDR5 WIN site inhibitor C16 and HDM2 antagonist Nutlin-3a act synergistically to inhibit proliferation of *SMARCB1*-deficient cancer cells. We further conclude that the mechanism of synergy is most likely due to enhanced p53 activation in response to dual inhibitor treatment in this context.

DISCUSSION

Discovering strategies to treat rhabdoid tumors is a challenging task. Not only are these cancers rare and aggressive, but because they are defined by loss of the *SMARCB1* tumor suppressor (3–5), they lack a clear and present oncogenic target for therapeutic intervention. Most likely, any practical regimen for RT will involve combinations of agents, making it imperative that we identify synergies that can inform how existing or future drugs can be used together to ameliorate these cancers. Here, we characterize how RT cells respond to a potent inhibitor of the WIN site of WDR5; representative of a novel class of inhibitors currently under development in multiple laboratories (22,25–29). We show that WIN site inhibitor evicts WDR5 from chromatin in RT cells, suppresses the expression of WDR5-bound genes connected to protein synthesis, and acts synergistically with HDM2 antagonists to induce p53 and block RT cell proliferation. This study strengthens the concept that WDR5 is a conserved regulator of genes connected to biomass accumulation, defines a predictable primary transcriptional response to WIN site inhibition, and provides a future rationale for the combined treatment of rhabdoid tumors with WDR5 and HDM2 inhibitors.

Our definition of the genomic binding sites of WDR5 in G401, KYM-1, and TTC549 cells reveals a pattern of chromatin association that is similar to what is seen in other contexts (21,24,30); a wide variation in binding site number across cell types, a tendency for WDR5 binding proximal to promoters, and inclusion of a set of ~100 genes that are bound by WDR5 in all cell types examined. These 100 common WDR5-bound genes are connected to protein synthesis and encode roughly half the protein subunits of the ribosome as well as nucleolar RNAs and translation factors. Although we do not yet understand the significance of this specific conserved pattern of WDR5 binding, we note that a majority of these genes are transcriptionally suppressed by WIN site inhibitor in RT, leukemia (21) and NB (24) cell lines, and by WDR5 degradation in NB cells (24), demonstrating that these genes are direct, bona-fide, and universal WDR5 targets. We also note that most of these genes are regulated by MYC in a WDR5-dependent manner in Ramos Burkitt lymphoma cells (30), suggesting that
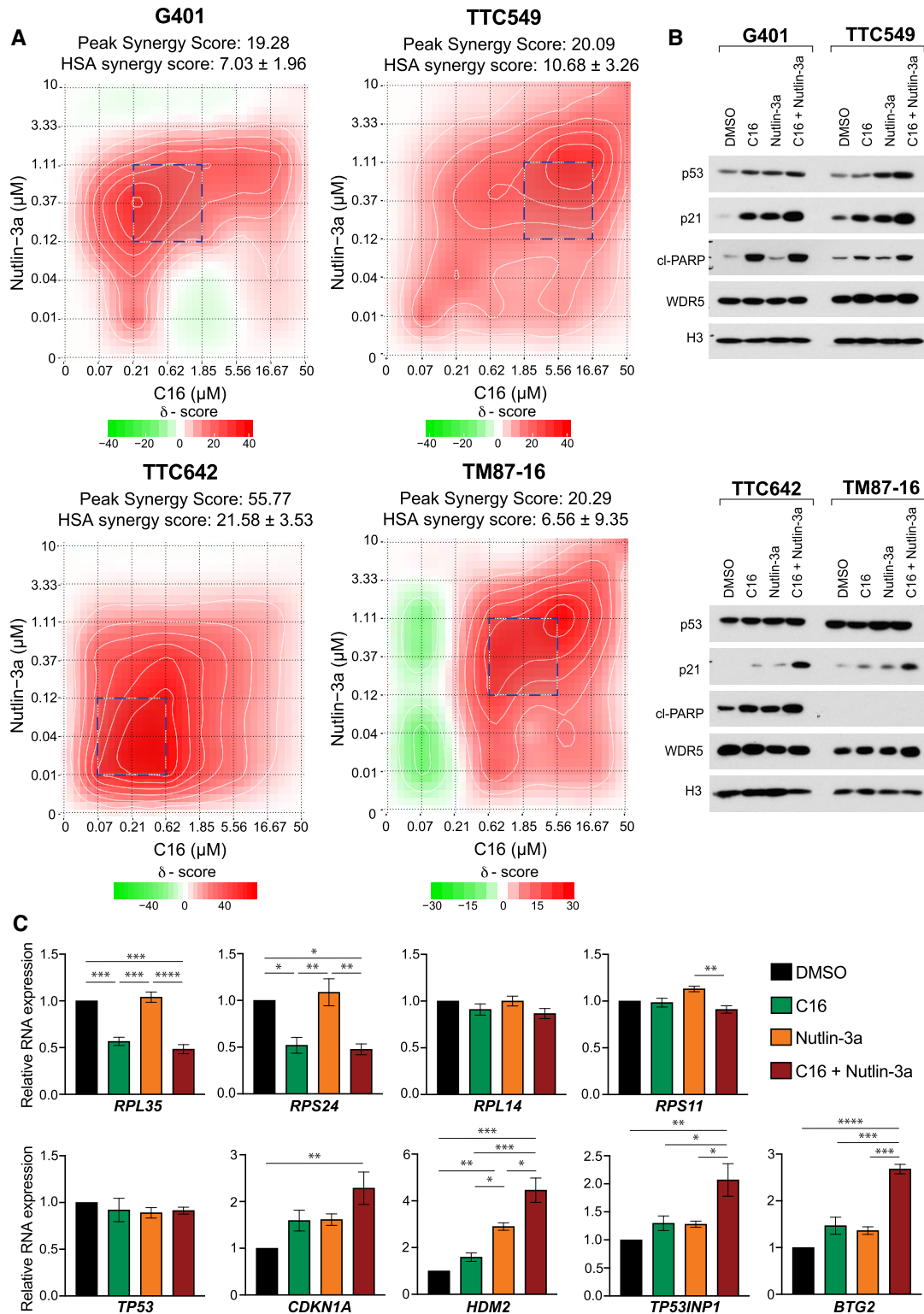
Figure 6. C16 synergizes with Nutlin-3a to induce p53 and inhibit proliferation of RT cells. (**A**) Synergy maps, as well as peak and average HSA scores for C16 and Nutlin-3a dose combinations ranging from 14 nM to 10 μM Nutlin-3a and 69 nM to 50 μM C16 in G401, TTC549, TTC642, and TM87-16 cells. Five day treatment ($n = 3$). HSA synergy score represents average HSA score of all dose combinations whereas peak synergy score represents the maximum average score for a three-by-three dose matrix within each map (indicated by dashed-line boxes). (**B**) Western blot, performed on lysates from cell lines that were treated with DMSO, 500 nM C16, 500 nM Nutlin-3a, or 500 nM C16 and Nutlin-3a for three days. Blots were probed with antibodies against the indicated proteins. 'cl-PARP' refers to cleaved PARP. Histone H3 is a loading control. Image is representative of three biological replicates. (**C**) RT-qPCR analysis of the indicated mRNA levels in TTC549 cells collected following treatment with DMSO, 500 nM C16, 500 nM Nutlin-3a, or 500 nM C16 and Nutlin-3a for 3 days. RNA expression shown relative to DMSO. *$P = <0.05$, ** $P = <0.01$, *** $P = <0.001$, **** $P = <0.0001$, as determined by ANOVA ($n = 3$, mean ± SEM).

the function of WDR5 at these universal target sites may be dedicated to the actions of MYC.

In RT cells, WIN site inhibitor results in the comprehensive displacement of WDR5 from chromatin, consistent with earlier reports that the integrity of the WIN site is essential for tethering WDR5 to its chromosomal locations (21,24,30). What is interesting, however, is that despite the widespread eviction of WDR5 from chromatin by C16, most genes bound by WDR5 do not respond to WIN site blockade, either early or over the course of days. This phenomenon is most clearly illustrated in KYM-1 cells, in which we track ∼700 WDR5 binding sites by ChIP-Seq but observe only 71 genes with altered transcription, as measured by PRO-Seq. The number of WDR5-bound genes that are transcriptionally impacted by WIN site inhibitor does increase somewhat by day three, but the vast majority of WDR5-bound genes are unresponsive during extended treatment, and conversely most of the transcriptional changes occur at genes that are not physically linked to WDR5. The disconnect between WDR5 binding and transcriptional response suggests that the function of WDR5 at most of its chromatin-binding sites is not measurable under our conditions. It is possible that these are 'storage' sites for WDR5, or are poised for induction in response to a specific signal. Alternatively, these binding sites may serve to bookmark genes for early reactivation after mitosis; a function previously described for WDR5 in human embryonic stem cells (67). Further investigation of this phenomenon are needed.

A number of important conclusions can be drawn from monitoring the activity of WIN site inhibitor C16 across a panel of *SMARCB1*-deficient cell lines. Despite a common genetic (MRT and AT/RT) or functional (synovial sarcoma) perturbation, these lines differ widely in their sensitivity to WIN site inhibitors. G401 and TTC642 cells, for example, are almost as sensitive to C6 and C16 as MV4;11 leukemia cells, which are often considered the prototype for a WIN site inhibitor-sensitive cell line (21,25). TTC549 and TM87-16 cells, in contrast, display IC$_{50}$ values close to those obtained in K562 cells (21,22), which we and others classified as least sensitive to WIN site inhibition. Previously, it has been challenging to know if a differential response to WIN site inhibitors is due to differences in intracellular compound accumulation or access to WDR5, but our use of the RPG target engagement assay demonstrates that differences in the extent of WDR5 inhibition do not underly the wide differential in cellular response across the panel. Rather, it appears as though WDR5 inhibition, as quantified by RPG transcription, is fairly consistent in all cell types, as is the precise set of genes that respond early to C16 in our PRO-Seq assays. Indeed, given the discrepancy in WDR5 binding events between G401 and KYM-1 cells, and their inherently diverse transcriptomes, it is intriguing to see how similar the primary transcriptional responses to C16 are between the two lines. Again, the majority of these primary target genes are WDR5-bound RPGs, which we know respond rapidly to earlier generation WIN site inhibitors in other cancer cell contexts (21,24). Like the conserved WDR5 binding sites, we suggest that there is a conserved set of protein synthesis genes broadly impacted by WIN site inhibitor in diverse cellular settings. Because

the pattern of WDR5 binding and the impact of WIN site inhibition is similar across sensitive and insensitive lines, it is not unreasonable to suggest that this response is universal and highly predictable, and that whether cells succumb or survive in response to WIN site inhibition has little to do with differences in how WDR5 and WIN site inhibitors act, but is instead determined by how cells respond to perturbations in the expression of these specific PSGs.

One determinant of an effective response to WIN site inhibition, based on earlier studies in leukemia (21) and NB (24) cells, is the presence of wild-type p53, which is induced by the ribosomal stress caused by alterations in RPG transcription (21). It is clear from our transcriptomic analyses that p53 target genes are induced in most RT lines in response to C16 treatment, which is consistent with earlier observations in MLLr and NB cells (21,24). What is surprising in RT cells, however, is that p53 is not consistently induced at the bulk protein level by C16, and is dispensable for the cellular impact of WIN site inhibitors. Precisely how WIN site inhibition results in robust activation of p53 in some cancer cell types, and not in the RT setting, is unclear, and although *TP53*-independent responses to ribosome perturbation/nucleolar stress have been described (68), they are mechanistically opaque. Understanding how RT cells respond to WIN site inhibition in the absence of p53, and why p53 is not robustly induced by WIN site inhibitor in this context, will require further investigation. Regardless of the mechanism, however, our findings here demonstrate that—contrary to our initial postulate (21)—cancer cells can respond to WIN site inhibition in the absence of functional p53. It may thus be possible to identify additional cancer cell types, bereft of p53, that are inhibited by WIN site blockade. If this forecast is correct, WIN site inhibitors could have much broader utility as anti-cancer agents than first imagined.

Perhaps the most significant implication of the p53-independence of the response of RT cells to WIN site inhibitor is that can be exploited to develop a combination inhibitor strategy centered on dual WDR5 and HDM2 inhibition. Based on our findings, we propose that the extent of p53 induction by C16 in RT cells, although detectable by RNA-Seq, is too small to affect a cellular outcome in this context. We further propose that this modest level of p53 induction is enhanced by HDM2 inhibition, resulting in the synergistic activation of p53 target genes and synergism in terms of cellular growth response. It is important to note that synergy occurs not only in our most sensitive RT lines, but also in some of the least sensitive lines, indicating that differences in response to WIN site inhibitor can be overcome when combined with an HDM2 antagonist. HDM2 inhibitors have not yet succeeded in clinical trials, likely due to a combination of acquisition of resistance, toxicities, and inability as a single agent to reliably trigger apoptosis in cancer cells (69). And WIN site inhibitors are as yet untested in terms of their *in vivo* efficacy, safety, or therapeutic window. But synergistic combination approaches—as we demonstrate here with HDM2 and WDR5 inhibitors—have the potential to overcome limiting factors associated with single agent therapies, and should allow each agent to be used at lower doses in a combination regimen. The near universal retention of p53 in RT, together with insight we pro-

vide here into how WIN site inhibitors act in RT cells, lays the foundation for future preclinical evaluation of WDR5 and HDM2 inhibitor combinations for treatment of deadly rhabdoid tumors.

DATA AVAILABILITY

Genomic data sets have been deposited at the Gene Expression Omnibus (GEO) at GSE173207 and GSE189205. Flow cytometry data have been deposited at the FLOW Repository (ID: FR-FCM-Z46Y and FR-FCM-Z4TM).

SUPPLEMENTARY DATA

Supplementary Data are available at NAR Cancer Online.

REFERENCES

1. Pawel,B.R. (2018) SMARCB1-deficient Tumors of Childhood: A Practical Guide. *Pediatr. Dev. Pathol.*, **21**, 6–28.
2. Fruhwald,M.C., Biegel,J.A., Bourdeaut,F., Roberts,C.W. and Chi,S.N. (2016) Atypical teratoid/rhabdoid tumors-current concepts, advances in biology, and potential future therapies. *Neuro. Oncol.*, **18**, 764–778.
3. Hasselblatt,M., Isken,S., Linge,A., Eikmeier,K., Jeibmann,A., Oyen,F., Nagel,I., Richter,J., Bartelheim,K., Kordes,U. *et al.* (2013) High-resolution genomic analysis suggests the absence of recurrent genomic alterations other than SMARCB1 aberrations in atypical teratoid/rhabdoid tumors. *Genes Chromosomes Cancer*, **52**, 185–190.
4. Hoell,J.I., Gombert,M., Bartenhagen,C., Ginzel,S., Husemann,P., Felsberg,J., Reifenberger,G., Eggert,A., Dugas,M., Schonberger,S. *et al.* (2013) Whole-genome paired-end analysis confirms remarkable genomic stability of atypical teratoid/rhabdoid tumors. *Genes Chromosomes Cancer*, **52**, 983–985.
5. Lee,R.S., Stewart,C., Carter,S.L., Ambrogio,L., Cibulskis,K., Sougnez,C., Lawrence,M.S., Auclair,D., Mora,J., Golub,T.R. *et al.* (2012) A remarkably simple genome underlies highly malignant pediatric rhabdoid cancers. *J. Clin. Invest.*, **122**, 2983–2988.
6. Roberts,C.W., Galusha,S.A., McMenamin,M.E., Fletcher,C.D. and Orkin,S.H. (2000) Haploinsufficiency of Snf5 (integrase interactor 1) predisposes to malignant rhabdoid tumors in mice. *Proc. Natl. Acad. Sci. U. S. A.*, **97**, 13796–13800.
7. Kim,K.H. and Roberts,C.W. (2014) Mechanisms by which SMARCB1 loss drives rhabdoid tumor growth. *Cancer Genet.*, **207**, 365–372.
8. Wang,X., Lee,R.S., Alver,B.H., Haswell,J.R., Wang,S., Mieczkowski,J., Drier,Y., Gillespie,S.M., Archer,T.C., Wu,J.N. *et al.* (2017) SMARCB1-mediated SWI/SNF complex function is essential for enhancer regulation. *Nat. Genet.*, **49**, 289–295.
9. Nakayama,R.T., Pulice,J.L., Valencia,A.M., McBride,M.J., McKenzie,Z.M., Gillespie,M.A., Ku,W.L., Teng,M., Cui,K., Williams,R.T. *et al.* (2017) SMARCB1 is required for widespread BAF complex-mediated activation of enhancers and bivalent promoters. *Nat. Genet.*, **49**, 1613–1623.
10. Alver,B.H., Kim,K.H., Lu,P., Wang,X., Manchester,H.E., Wang,W., Haswell,J.R., Park,P.J. and Roberts,C.W. (2017) The SWI/SNF chromatin remodelling complex is required for maintenance of lineage specific enhancers. *Nat. Commun.*, **8**, 14648.
11. Michel,B.C., D'Avino,A.R., Cassel,S.H., Mashtalir,N., McKenzie,Z.M., McBride,M.J., Valencia,A.M., Zhou,Q., Bocker,M., Soares,L.M.M. *et al.* (2018) A non-canonical SWI/SNF complex is a synthetic lethal target in cancers driven by BAF complex perturbation. *Nat. Cell Biol.*, **20**, 1410–1420.
12. Wang,X., Wang,S., Troisi,E.C., Howard,T.P., Haswell,J.R., Wolf,B.K., Hawk,W.H., Ramos,P., Oberlick,E.M., Tzvetkov,E.P. *et al.* (2019) BRD9 defines a SWI/SNF sub-complex and constitutes a specific vulnerability in malignant rhabdoid tumors. *Nat. Commun.*, **10**, 1881.
13. Weissmiller,A.M., Wang,J., Lorey,S.L., Howard,G.C., Martinez,E., Liu,Q. and Tansey,W.P. (2019) Inhibition of MYC by the SMARCB1 tumor suppressor. *Nat. Commun.*, **10**, 2014.
14. Woodley,C.M., Romer,A.S., Wang,J., Guarnaccia,A.D., Elion,D.L., Maxwell,J.N., Guerrazzi,K., McCann,T.S., Popay,T.M., Matlock,B.K. *et al.* (2021) Multiple interactions of the oncoprotein transcription factor MYC with the SWI/SNF chromatin remodeler. *Oncogene*, **40**, 3593–3609.
15. Gadd,S., Sredni,S.T., Huang,C.C., Perlman,E.J. and Renal Tumor Committee of the Children's Oncology, G. (2010) Rhabdoid tumor: gene expression clues to pathogenesis and potential therapeutic targets. *Lab. Invest.*, **90**, 724–738.
16. Wang,X., Werneck,M.B., Wilson,B.G., Kim,H.J., Kluk,M.J., Thom,C.S., Wischhusen,J.W., Evans,J.A., Jesneck,J.L., Nguyen,P. *et al.* (2011) TCR-dependent transformation of mature memory phenotype T cells in mice. *J. Clin. Invest.*, **121**, 3834–3845.
17. Genovese,G., Carugo,A., Tepper,J., Robinson,F.S., Li,L., Svelto,M., Nezi,L., Corti,D., Minelli,R., Pettazzoni,P. *et al.* (2017) Synthetic vulnerabilities of mesenchymal subpopulations in pancreatic cancer. *Nature*, **542**, 362–366.
18. Carugo,A., Minelli,R., Sapio,L., Soeung,M., Carbone,F., Robinson,F.S., Tepper,J., Chen,Z., Lovisa,S., Svelto,M. *et al.* (2019)

p53 is a Master Regulator of Proteostasis in SMARCB1-Deficient Malignant Rhabdoid Tumors. *Cancer Cell*, **35**, 204–220.

19. Johann,P.D., Erkek,S., Zapatka,M., Kerl,K., Buchhalter,I., Hovestadt,V., Jones,D.T., Sturm,D., Hermann,C., Segura Wang,M. *et al.* (2016) Atypical Teratoid/Rhabdoid Tumors Are Comprised of Three Epigenetic Subgroups with Distinct Enhancer Landscapes. *Cancer Cell*, **29**, 379–393.

20. Wang,F., Jeon,K.O., Salovich,J.M., Macdonald,J.D., Alvarado,J., Gogliotti,R.D., Phan,J., Olejniczak,E.T., Sun,Q., Wang,S. *et al.* (2018) Discovery of Potent 2-Aryl-6,7-Dihydro-5 H-Pyrrolo[1,2-a]imidazoles as WDR5 WIN-site Inhibitors Using Fragment-Based Methods and Structure-Based Design. *J. Med. Chem.*, **61**, 5623–5642.

21. Aho,E.R., Wang,J., Gogliotti,R.D., Howard,G.C., Phan,J., Acharya,P., Macdonald,J.D., Cheng,K., Lorey,S.L., Lu,B. *et al.* (2019) Displacement of WDR5 from Chromatin by a WIN Site Inhibitor with Picomolar Affinity. *Cell Rep.*, **26**, 2916–2928.

22. Tian,J., Teuscher,K.B., Aho,E.R., Alvarado,J.R., Mills,J.J., Meyers,K.M., Gogliotti,R.D., Han,C., Macdonald,J.D., Sai,J. *et al.* (2020) Discovery and Structure-Based Optimization of Potent and Selective WD Repeat Domain 5 (WDR5) Inhibitors Containing a Dihydroisoquinolinone Bicyclic Core. *J. Med. Chem.*, **63**, 656–675.

23. Guarnaccia,A.D. and Tansey,W.P. (2018) Moonlighting with WDR5: A Cellular Multitasker. *J Clin Med*, **7**, 21–37.

24. Bryan,A.F., Wang,J., Howard,G.C., Guarnaccia,A.D., Woodley,C.M., Aho,E.R., Rellinger,E.J., Matlock,B.K., Flaherty,D.K., Lorey,S.L. *et al.* (2020) WDR5 is a conserved regulator of protein synthesis gene expression. *Nucleic. Acids. Res.*, **48**, 2924–2941.

25. Cao,F., Townsend,E.C., Karatas,H., Xu,J., Li,L., Lee,S., Liu,L., Chen,Y., Ouillette,P., Zhu,J. *et al.* (2014) Targeting MLL1 H3K4 methyltransferase activity in mixed-lineage leukemia. *Mol. Cell*, **53**, 247–261.

26. Grebien,F., Vedadi,M., Getlik,M., Giambruno,R., Grover,A., Avellino,R., Skucha,A., Vittori,S., Kuznetsova,E., Smil,D. *et al.* (2015) Pharmacological targeting of the Wdr5-MLL interaction in C/EBPalpha N-terminal leukemia. *Nat. Chem. Biol.*, **11**, 571–578.

27. Li,D.D., Chen,W.L., Xu,X.L., Jiang,F., Wang,L., Xie,Y.Y., Zhang,X.J., Guo,X.K., You,Q.D. and Sun,H.P. (2016) Structure-based design and synthesis of small molecular inhibitors disturbing the interaction of MLL1-WDR5. *Eur. J. Med. Chem.*, **118**, 1–8.

28. Karatas,H., Li,Y., Liu,L., Ji,J., Lee,S., Chen,Y., Yang,J., Huang,L., Bernard,D., Xu,J. *et al.* (2017) Discovery of a Highly Potent, Cell-Permeable Macrocyclic Peptidomimetic (MM-589) Targeting the WD Repeat Domain 5 Protein (WDR5)-Mixed Lineage Leukemia (MLL) Protein-Protein Interaction. *J. Med. Chem.*, **60**, 4818–4839.

29. Zhang,X., Zheng,X., Yang,H., Yan,J., Fu,X., Wei,R., Xu,X., Zhang,Z., Yu,A., Zhou,K. *et al.* (2018) Piribedil disrupts the MLL1-WDR5 interaction and sensitizes MLL-rearranged acute myeloid leukemia (AML) to doxorubicin-induced apoptosis. *Cancer Lett.*, **431**, 150–160.

30. Thomas,L.R., Adams,C.M., Wang,J., Weissmiller,A.M., Creighton,J., Lorey,S.L., Liu,Q., Fesik,S.W., Eischen,C.M. and Tansey,W.P. (2019) Interaction of the oncoprotein transcription factor MYC with its chromatin cofactor WDR5 is essential for tumor maintenance. *Proc. Natl. Acad. Sci. U. S. A.*, **116**, 25260–25268.

31. Howard,T.P., Oberlick,E.M., Rees,M.G., Arnoff,T.E., Pham,M.T., Brenan,L., DoCarmo,M., Hong,A.L., Kugener,G., Chou,H.C. *et al.* (2020) Rhabdoid Tumors Are Sensitive to the Protein-Translation Inhibitor Homoharringtonine. *Clinical Cancer Research: An Official Journal of the American Association for Cancer Research*, **26**, 4995–5006.

32. Howard,T.P., Arnoff,T.E., Song,M.R., Giacomelli,A.O., Wang,X., Hong,A.L., Dharia,N.V., Wang,S., Vazquez,F., Pham,M.T. *et al.* (2019) MDM2 and MDM4 Are Therapeutic Vulnerabilities in Malignant Rhabdoid Tumors. *Cancer Res.*, **79**, 2404–2414.

33. Kim,J.S., Lee,C., Bonifant,C.L., Ressom,H. and Waldman,T. (2007) Activation of p53-dependent growth suppression in human cells by mutations in PTEN or PIK3CA. *Mol. Cell. Biol.*, **27**, 662–677.

34. Sarbassov,D.D., Guertin,D.A., Ali,S.M. and Sabatini,D.M. (2005) Phosphorylation and regulation of Akt/PKB by the rictor-mTOR complex. *Science*, **307**, 1098–1101.

35. Sanson,K.R., Hanna,R.E., Hegde,M., Donovan,K.F., Strand,C., Sullender,M.E., Vaimberg,E.W., Goodale,A., Root,D.E., Piccioni,F. *et al.* (2018) Optimized libraries for CRISPR-Cas9 genetic screens with multiple modalities. *Nat. Commun.*, **9**, 5416.

36. Rosenbluh,J., Xu,H., Harrington,W., Gill,S., Wang,X., Vazquez,F., Root,D.E., Tsherniak,A. and Hahn,W.C. (2017) Complementary information derived from CRISPR Cas9 mediated gene deletion and suppression. *Nat. Commun.*, **8**, 15403.

37. Ianevski,A., He,L., Aittokallio,T. and Tang,J. (2017) SynergyFinder: a web application for analyzing drug combination dose-response matrix data. *Bioinformatics*, **33**, 2413–2415.

38. Tworkowski,K.A., Chakraborty,A.A., Samuelson,A.V., Seger,Y.R., Narita,M., Hannon,G.J., Lowe,S.W. and Tansey,W.P. (2008) Adenovirus E1A targets p400 to induce the cellular oncoprotein Myc. *Proc. Natl. Acad. Sci. U. S. A.*, **105**, 6103–6108.

39. An,H., Landis,J.T., Bailey,A.G., Marron,J.S. and Dittmer,D.P. (2019) dr4pl: a stable convergence algorithm for the 4 parameter logistic model. *The R Journal*, **11**, 171–190.

40. Feng,J., Liu,T., Qin,B., Zhang,Y. and Liu,X.S. (2012) Identifying ChIP-seq enrichment using MACS. *Nat. Protoc.*, **7**, 1728–1740.

41. Ross-Innes,C.S., Stark,R., Teschendorff,A.E., Holmes,K.A., Ali,H.R., Dunning,M.J., Brown,G.D., Gojis,O., Ellis,I.O., Green,A.R. *et al.* (2012) Differential oestrogen receptor binding is associated with clinical outcome in breast cancer. *Nature*, **481**, 389–393.

42. Love,M.I., Huber,W. and Anders,S. (2014) Moderated estimation of fold change and dispersion for RNA-seq data with DESeq2. *Genome Biol.*, **15**, 550.

43. Martin,M. (2011) Cutadapt Removes Adapter Sequences From High-Throughput Sequencing Reads. *EMBnet.journal*, **17**, 10–12.

44. Dobin,A., Davis,C.A., Schlesinger,F., Drenkow,J., Zaleski,C., Jha,S., Batut,P., Chaisson,M. and Gingeras,T.R. (2013) STAR: ultrafast universal RNA-seq aligner. *Bioinformatics*, **29**, 15–21.

45. Liao,Y., Smyth,G.K. and Shi,W. (2014) featureCounts: an efficient general purpose program for assigning sequence reads to genomic features. *Bioinformatics*, **30**, 923–930.

46. Langmead,B. and Salzberg,S.L. (2012) Fast gapped-read alignment with Bowtie 2. *Nat. Methods*, **9**, 357–359.

47. Wang,J., Zhao,Y., Zhou,X., Hiebert,S.W., Liu,Q. and Shyr,Y.. (2018) Nascent RNA sequencing analysis provides insights into enhancer-mediated gene regulation. *BMC Genomics*, **19**, 633.

48. Core,L.J., Waterfall,J.J. and Lis,J.T. (2008) Nascent RNA sequencing reveals widespread pausing and divergent initiation at human promoters. *Science*, **322**, 1845–1848.

49. Lange,B., Valtieri,M., Santoli,D., Caracciolo,D., Mavilio,F., Gemperlein,I., Griffin,C., Emanuel,B., Finan,J., Nowell,P. *et al.* (1987) Growth factor requirements of childhood acute leukemia: establishment of GM-CSF-dependent cell lines. *Blood*, **70**, 192–199.

50. Sonobe,H., Manabe,Y., Furihata,M., Iwata,J., Oka,T., Ohtsuki,Y., Mizobuchi,H., Yamamoto,H., Kumano,O. and Abe,S. (1992) Establishment and characterization of a new human synovial sarcoma cell line. *HS-SY-II. Lab Invest*, **67**, 498–505.

51. Yanagisawa,S., Kadouchi,I., Yokomori,K., Hirose,M., Hakozaki,M., Hojo,H., Maeda,K., Kobayashi,E. and Murakami,T. (2009) Identification and metastatic potential of tumor-initiating cells in malignant rhabdoid tumor of the kidney. *Clinical Cancer Research: An Official Journal of the American Association for Cancer Research*, **15**, 3014–3022.

52. Naka,N., Takenaka,S., Araki,N., Miwa,T., Hashimoto,N., Yoshioka,K., Joyama,S., Hamada,K., Tsukamoto,Y., Tomita,Y. *et al.* (2010) Synovial sarcoma is a stem cell malignancy. *Stem Cells*, **28**, 1119–1131.

53. Barretina,J., Caponigro,G., Stransky,N., Venkatesan,K., Margolin,A.A., Kim,S., Wilson,C.J., Lehar,J., Kryukov,G.V., Sonkin,D. *et al.* (2012) The Cancer Cell Line Encyclopedia enables predictive modelling of anticancer drug sensitivity. *Nature*, **483**, 603–607.

54. Xu,J., Erdreich-Epstein,A., Gonzalez-Gomez,I., Melendez,E.Y., Smbatyan,G., Moats,R.A., Rosol,M., Biegel,J.A. and Reynolds,C.P. (2012) Novel cell lines established from pediatric brain tumors. *J. Neurooncol.*, **107**, 269–280.

55. Tate,J.G., Bamford,S., Jubb,H.C., Sondka,Z., Beare,D.M., Bindal,N., Boutselakis,H., Cole,C.G., Creatore,C., Dawson,E. *et al.* (2019) COSMIC: the Catalogue Of Somatic Mutations In Cancer. *Nucleic. Acids. Res.*, **47**, D941–D947.

56. Kadoch,C. and Crabtree,G.R. (2013) Reversible disruption of mSWI/SNF (BAF) complexes by the SS18-SSX oncogenic fusion in synovial sarcoma. *Cell*, **153**, 71–85.

57. Bodnar,A.G., Ouellette,M., Frolkis,M., Holt,S.E., Chiu,C.P., Morin,G.B., Harley,C.B., Shay,J.W., Lichtsteiner,S. and Wright,W.E. (1998) Extension of life-span by introduction of telomerase into normal human cells. *Science*, **279**, 349–352.

58. Kwak,H., Fuda,N.J., Core,L.J. and Lis,J.T. (2013) Precise maps of RNA polymerase reveal how promoters direct initiation and pausing. *Science*, **339**, 950–953.

59. Wang,J., Zhao,Y., Zhou,X., Hiebert,S.W., Liu,Q. and Shyr,Y. (2018) Nascent RNA sequencing analysis provides insights into enhancer-mediated gene regulation. *BMC Genomics*, **19**, 633.

60. Bieging-Rolett,K.T., Kaiser,A.M., Morgens,D.W., Boutelle,A.M., Seoane,J.A., Van Nostrand,E.L., Zhu,C., Houlihan,S.L., Mello,S.S., Yee,B.A. *et al.* (2020) Zmat3 Is a Key Splicing Regulator in the p53 Tumor Suppression Program. *Mol. Cell*, **80**, 452–469.

61. Jassal,B., Matthews,L., Viteri,G., Gong,C., Lorente,P., Fabregat,A., Sidiropoulos,K., Cook,J., Gillespie,M., Haw,R. *et al.* (2020) The reactome pathway knowledgebase. *Nucleic. Acids. Res.*, **48**, D498–D503.

62. Signer,R.A., Magee,J.A., Salic,A. and Morrison,S.J. (2014) Haematopoietic stem cells require a highly regulated protein synthesis rate. *Nature*, **509**, 49–54.

63. Vassilev,L.T., Vu,B.T., Graves,B., Carvajal,D., Podlaski,F., Filipovic,Z., Kong,N., Kammlott,U., Lukacs,C., Klein,C. *et al.* (2004) In vivo activation of the p53 pathway by small-molecule antagonists of MDM2. *Science*, **303**, 844–848.

64. Fischer,M. (2017) Census and evaluation of p53 target genes. *Oncogene*, **36**, 3943–3956.

65. Berenbaum,M.C. (1989) What is synergy?*Pharmacol. Rev.*, **41**, 93–141.

66. Furet,P., Masuya,K., Kallen,J., Stachyra-Valat,T., Ruetz,S., Guagnano,V., Holzer,P., Mah,R., Stutz,S., Vaupel,A. *et al.* (2016) Discovery of a novel class of highly potent inhibitors of the p53-MDM2 interaction by structure-based design starting from a conformational argument. *Bioorg. Med. Chem. Lett.*, **26**, 4837–4841.

67. Oh,E., Mark,K.G., Mocciaro,A., Watson,E.R., Prabu,J.R., Cha,D.D., Kampmann,M., Gamarra,N., Zhou,C.Y. and Rape,M. (2020) Gene expression and cell identity controlled by anaphase-promoting complex. *Nature*, **579**, 136–140.

68. James,A., Wang,Y., Raje,H., Rosby,R. and DiMario,P. (2014) Nucleolar stress with and without p53. *Nucleus*, **5**, 402–426.

69. Mullard,A. (2020) p53 programmes plough on. *Nature Reviews Drug Discovery*, **19**, 497–500.